低维人工纳米结构的构筑及其新奇物性

顾长志

中科院物理所微加工实验室
北京凝聚态物理国家实验室微加工部

2009年4月2日

纳米材料的新颖物性

牛顿力学　　　　　　量子力学

宏观 ←费米波长 / 特征尺寸→ 纳米

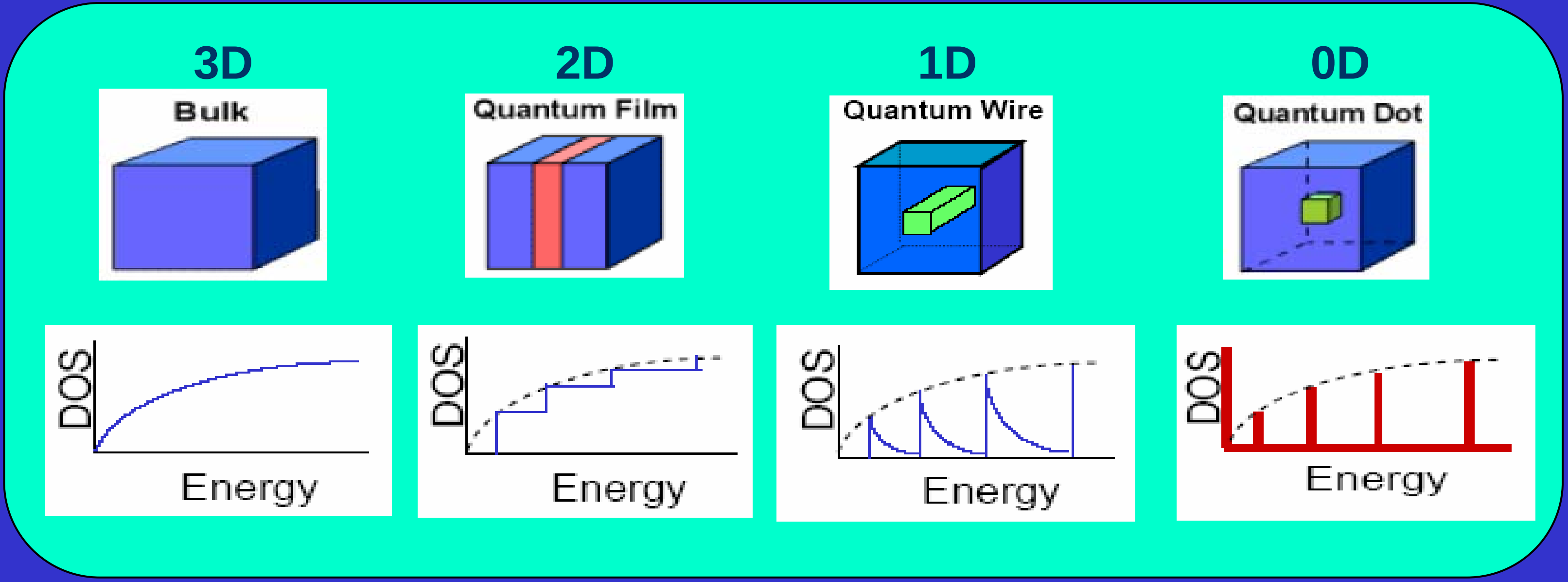

量子尺寸效应

- **影响材料性质的几个参数：**

  简并电子系统的费米波长（金属< 1nm、半导体: 几十nm）

  电子的平均自由程（几纳米—几十纳米）

  激子扩散长度（100nm左右）等

- **伴随的量子现象：**

  库仑阻塞(Coulomb Blockade)

  弹道输运(Ballistic Transport)等

- **物性的改变：**

  材料的电子结构、输运、磁学、光学和力学等物理性质均要发生明显的变化

- **问题：**

  性能对微观结构的敏感性

  材料体系的选择、生长的控制和微加工的精确程度

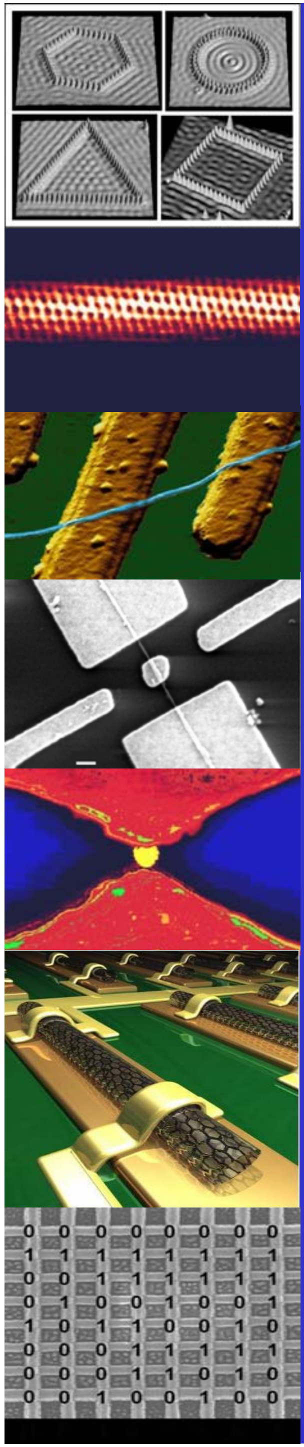

信息社会的发展需求

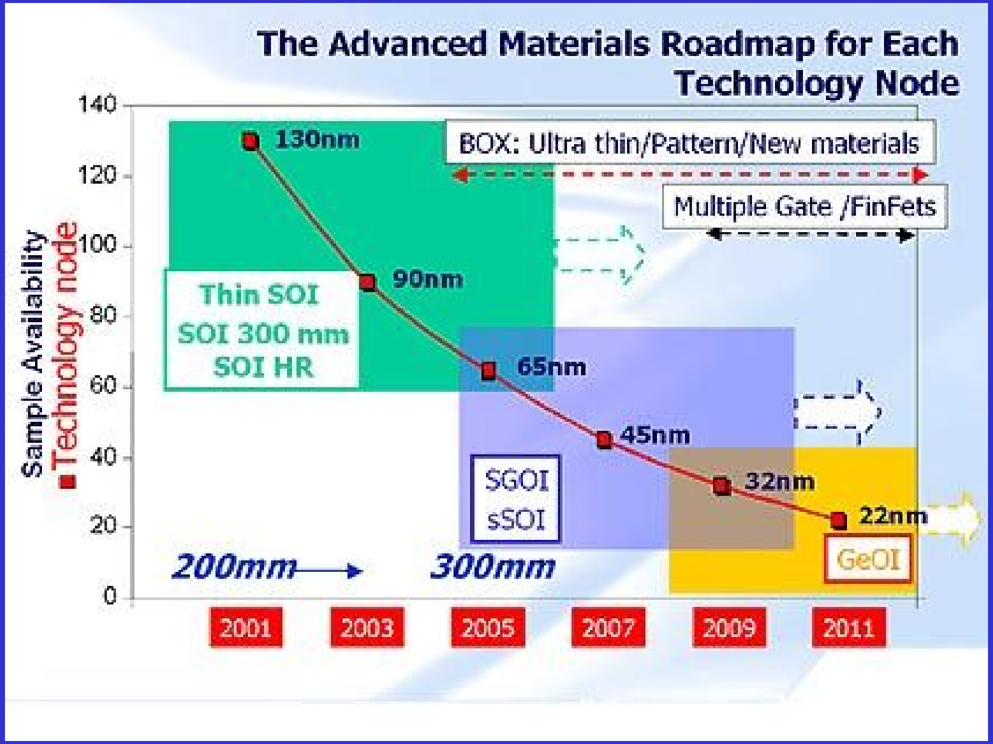

高可靠性电子材料
（第三代半导体材料）

→

小尺寸、大功率、耐高温、耐高压、抗辐射、抗腐蚀电子器件

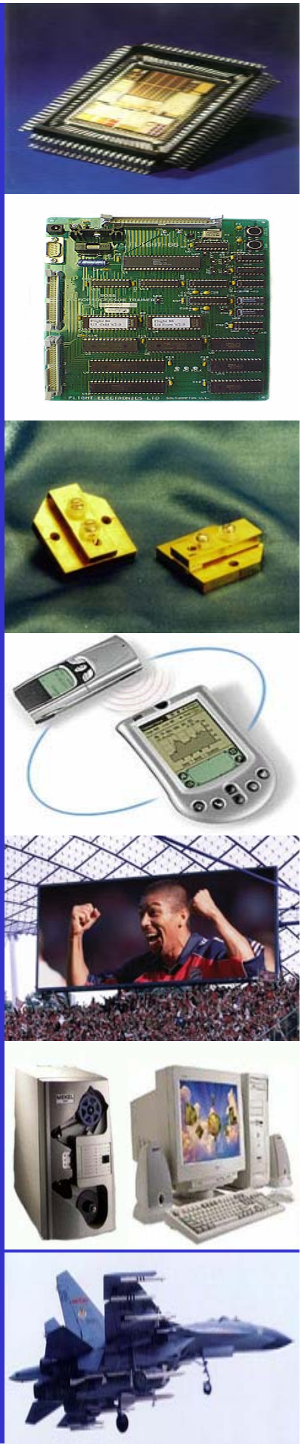

纳米科技面临的挑战

- How to control the identity, placement, and function of every important atom in a nanoscale solid？
- How to understand the systems that are too large to be handled by bruteforce calculation, but too small to be tackled by statistical methods?

A frontier science —— a mature discipline

- A revolutionary impact on fields from materials to information, and from energy to biology.

Fabrication of magnetic nanostructures

- **"Top Down"**

  well controlled in several tens nanometer

- **"Bottom up"**

  an art rather than a technology

微纳加工技术

- 在衬底表面用图形曝光和图形转移的方法制备出微/纳米尺度图形结构的过程

- 包括:

  曝光技术

  图形转移技术（刻蚀或剥离）

微纳米加工技术的分类

- 平面工艺：平行加工

  光源：紫外、极紫外、X射线、电子束、离子束、激光束

- 探针工艺：顺序加工

  固态探针：STM、AFM探针

  非固态探针：聚焦离子束、电子束、原子束、激光束等

- 模型工艺

  纳米压印、塑料模压、模铸技术

Laboratory of Microfabrication

Photolithography

MA6 mask aligner

- resolution: < 0.5μm
  @vacuum contact
- mask size: up to 6”
- substrate size: up to 6”
- alignment: two-side
  infrared

Overview of Align/Expose/Develop Steps

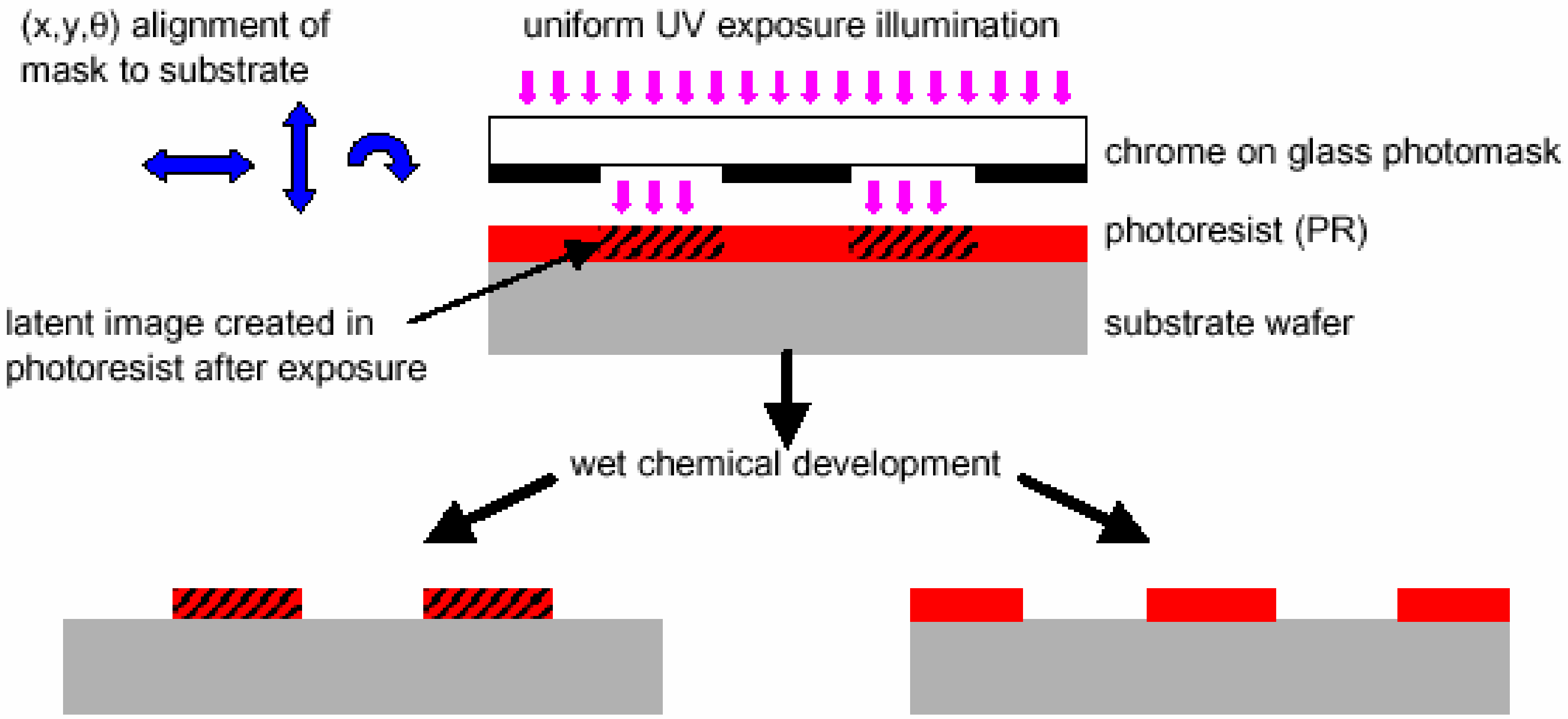

(x,y,θ) alignment of
mask to substrate

uniform UV exposure illumination

chrome on glass photomask

photoresist (PR)

substrate wafer

latent image created in
photoresist after exposure

wet chemical development

NEGATIVE PHOTORESIST

Photoresist is photopolymerized where exposed and rendered insoluble to the developer solution.

POSITIVE PHOTORESIST

Exposure decomposes a development inhibitor and developer solution only dissolves photoresist in the exposed areas.

Typical Results of MA6

Resolution: < 0.5 micrometer

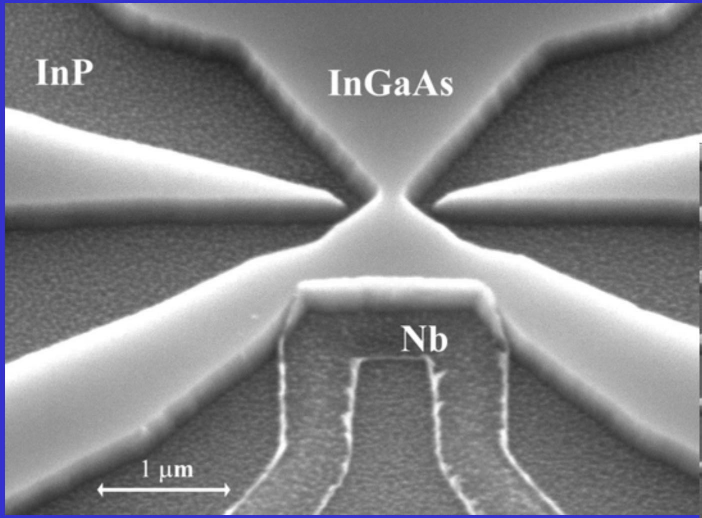

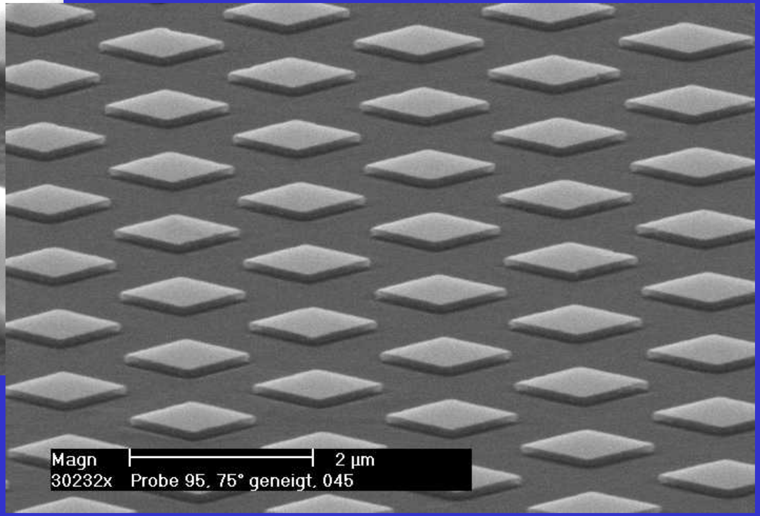

分辨率$R=k\cdot\lambda/NA$

Electron Beam Lithography

Raith150

- High voltage: 0.2kV~30kV
- Resolution: 50 nm
- Stitching: 20 nm
- Overlay: 20 nm

电子束曝光系统

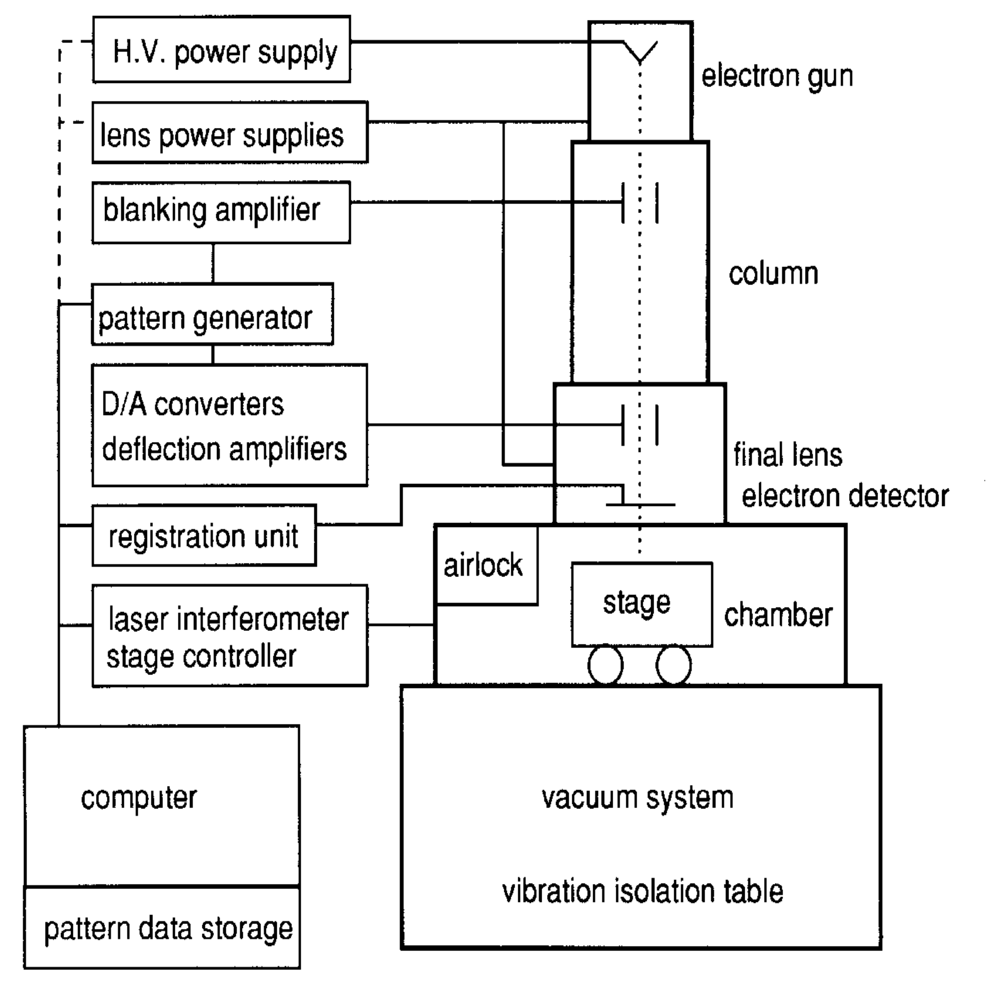

电子的波长为:

$$L = 1.2/(V_b)^{1/2}\ nm$$

（在25kV约为0.008 nm）

Focused Ion Beam Lithography

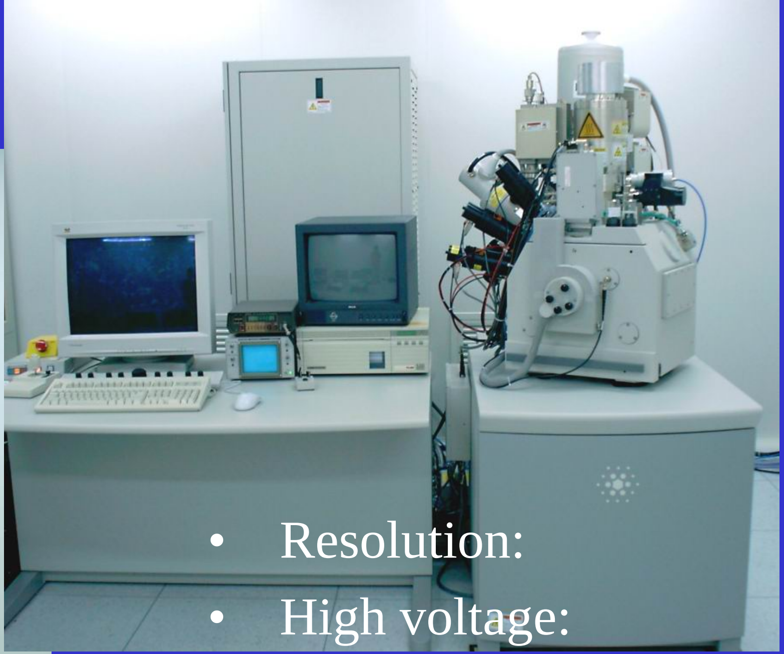

• Resolution:	5 nm
• High voltage:	8kV~30kV
• Motorized stage:	6 axes
• Function:	etching deposition

Typical Results of FIB

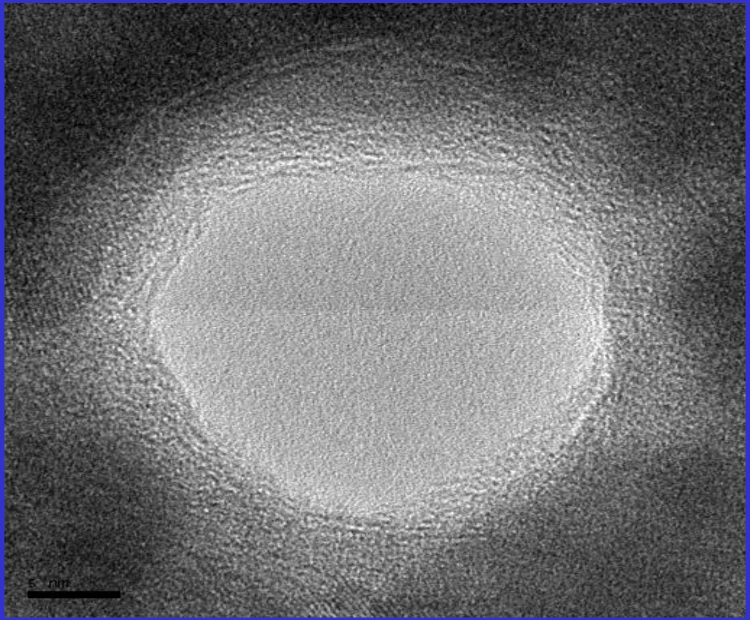

Ion beam resolution: 5 nm

The minimum line width: 10 nm

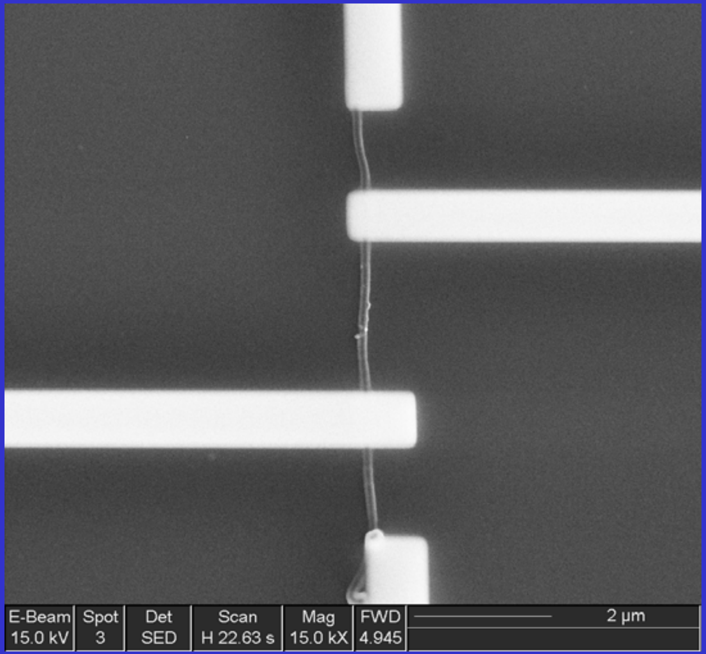

FIB/SEM

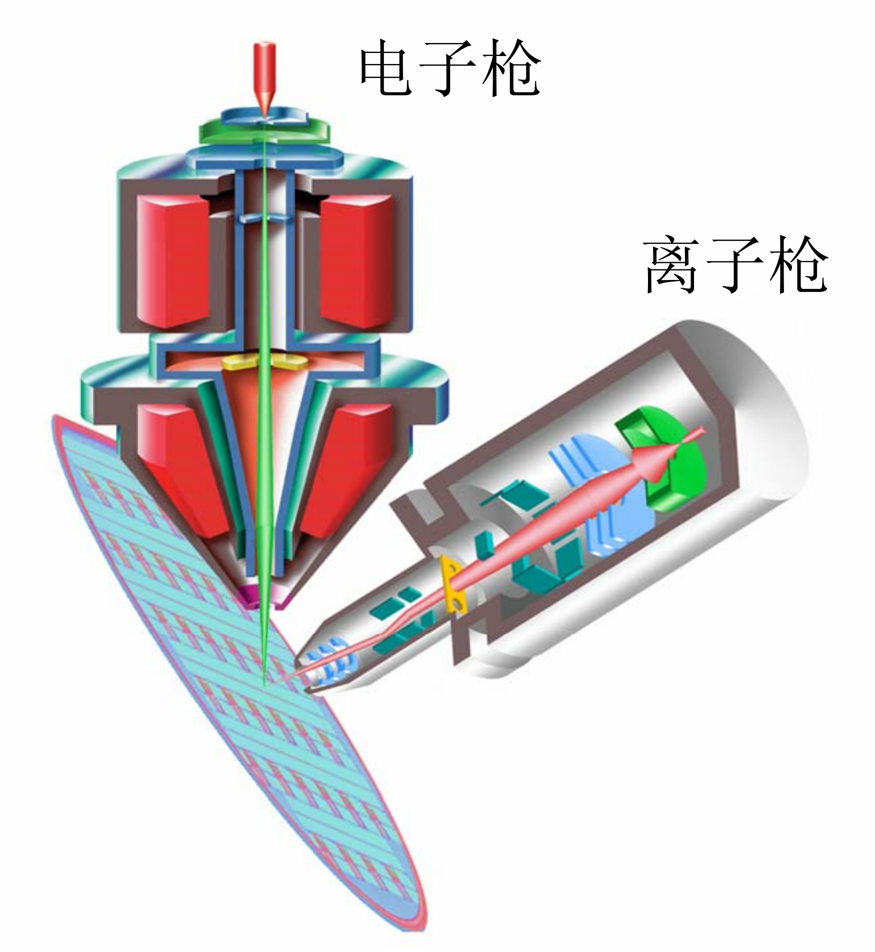

气体注入系统

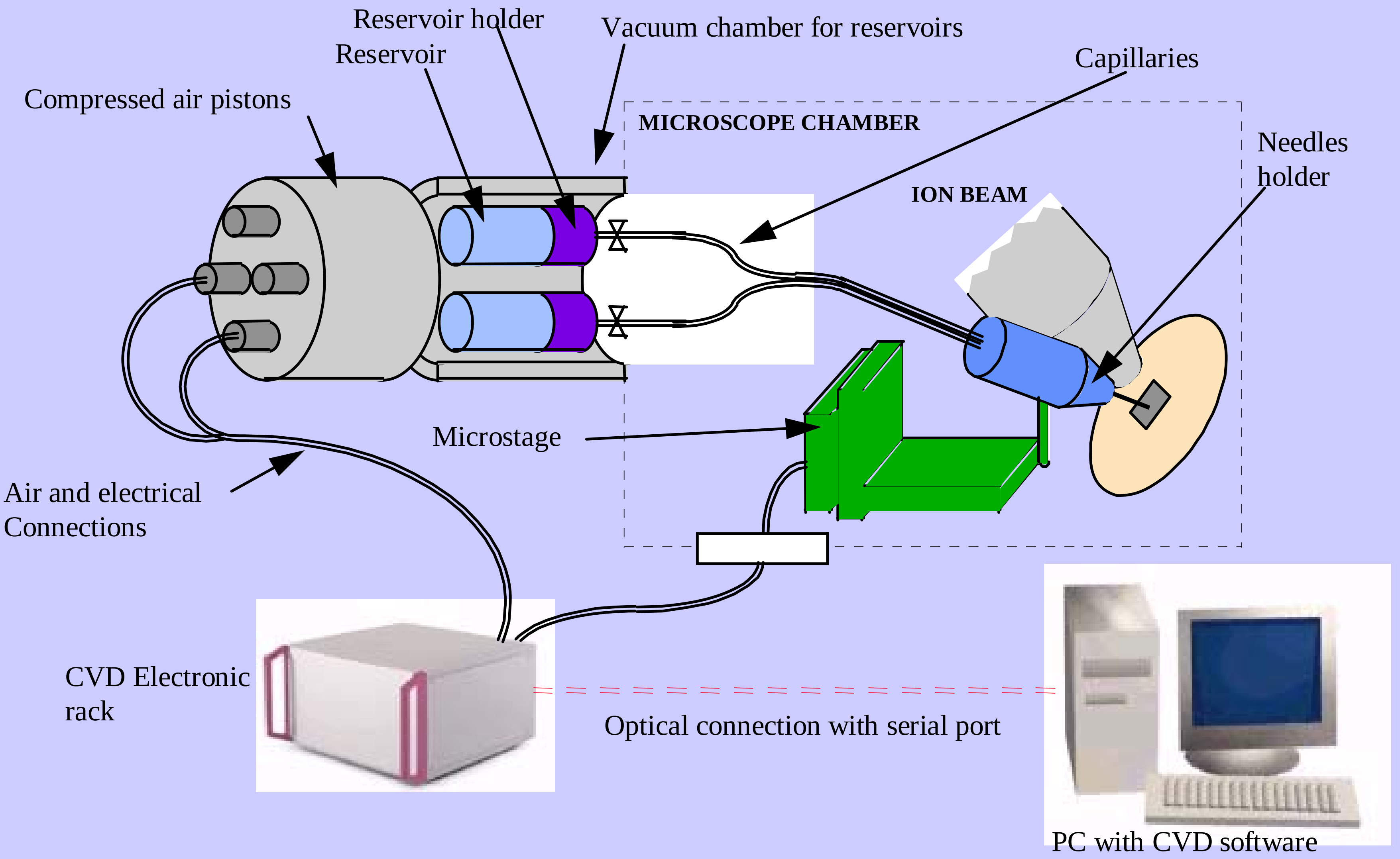
Reservoir holder
Reservoir
Vacuum chamber for reservoirs
Compressed air pistons
Capillaries
MICROSCOPE CHAMBER
Needles holder
ION BEAM
Microstage
Air and electrical Connections
CVD Electronic rack
Optical connection with serial port
PC with CVD software

Operating Principle of FIB

1. Ion-solid interaction

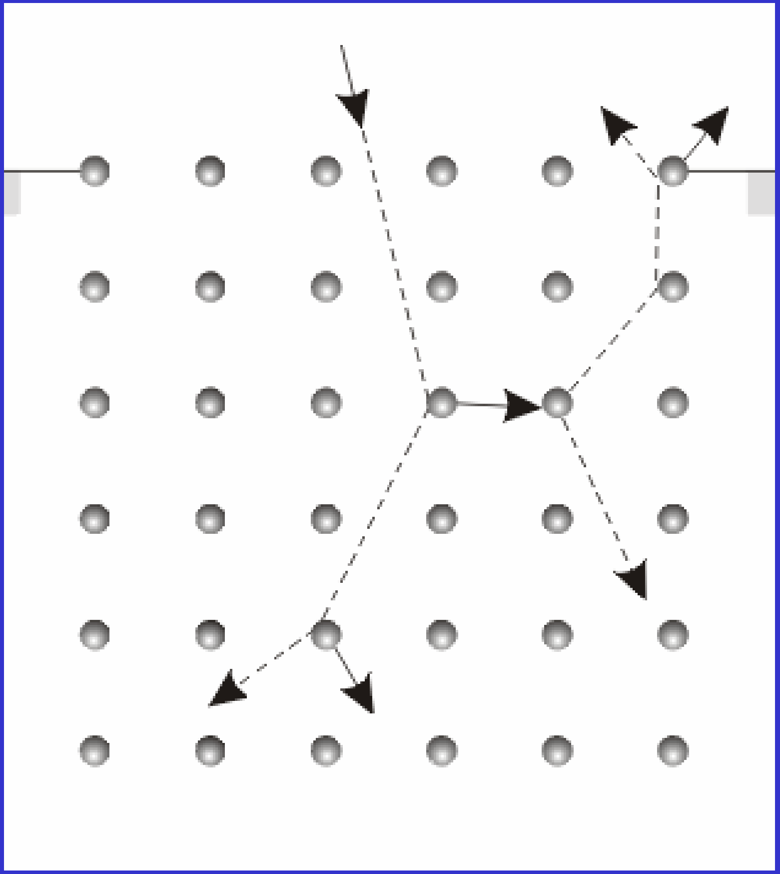

The primary ion produces a linear collision cascade, in which almost only binary collisions occur. Due to this cascade, energy can be transferred back to the surface. If more energy than the surface-binding-energy is placed upon a surface atom, it can be removed from the sample. The average number of atoms removed by one primary ion is called sputter yield (Y). It is strongly depended on the material, ion energy, incidence angle and environmental conditions.

2. Basics of beam deposition (Pt)

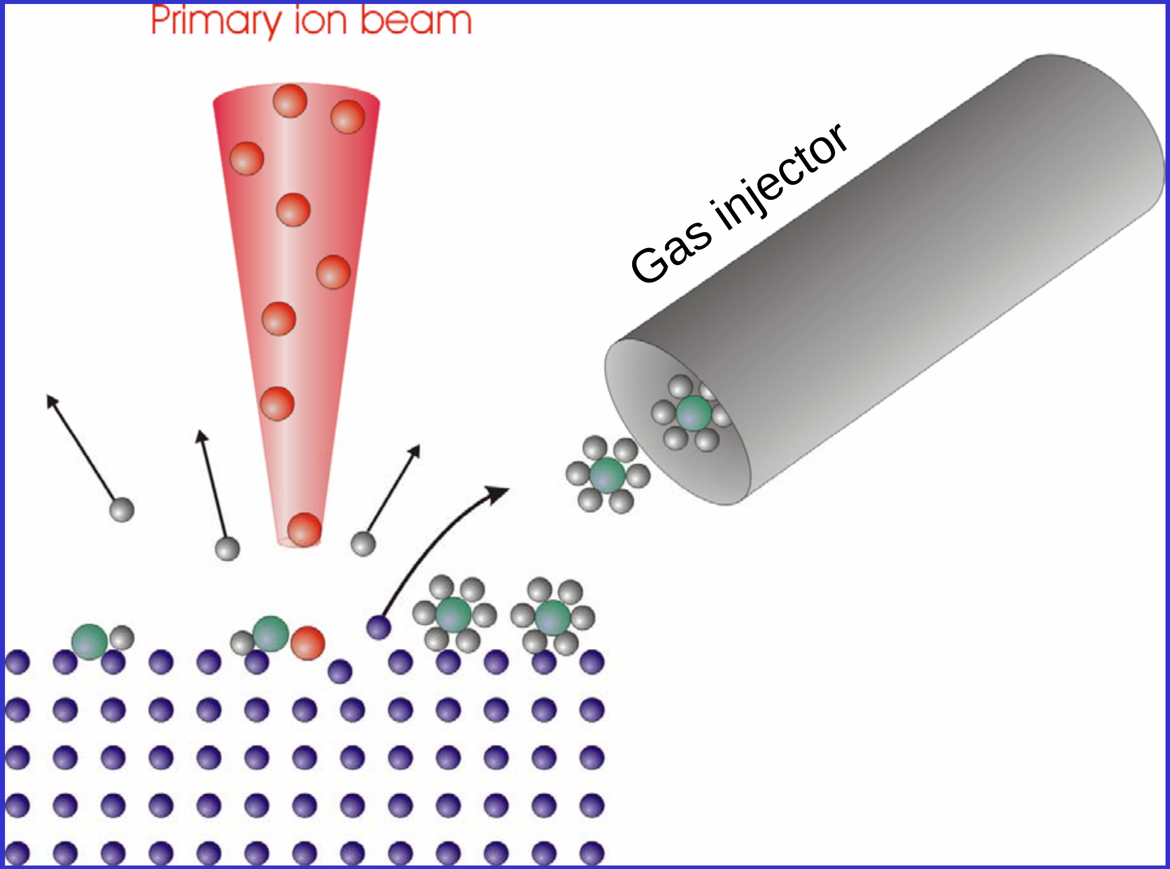

A heated capillary is used to inject a precursor gas eg. $Pt(CO)_6$ (Platinum-hexacarbonyl) nearby the beam. Due to the particle beam (either electrons or ions) energy is deposited onto the precursor molecule. The molecule decomposes and the metal atom is bound to the surface.

The applications of FIB

- cross-sectional imaging through semiconductor devices (or any layered structure)
- modification of the electrical routing on semiconductor devices
- failure analysis
- mask repair
- preparation for physical-chemical analysis
- preparation of specimens for transmission electron microscopy (TEM)
- Micro/nano-machining

Local cut and connection

- Device modification (2 cuts and 1 metal deposition)

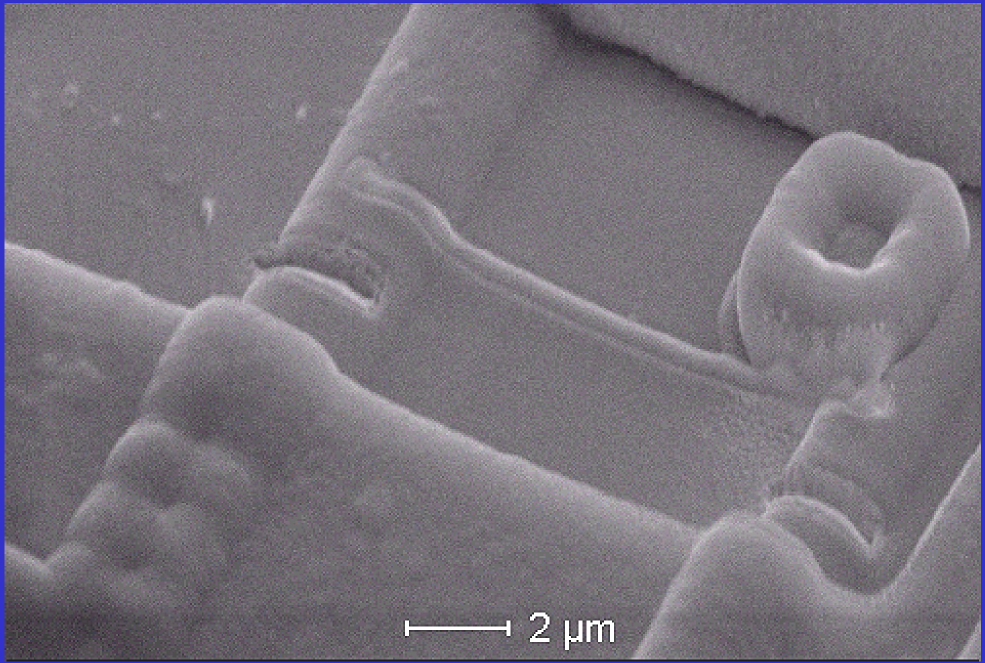

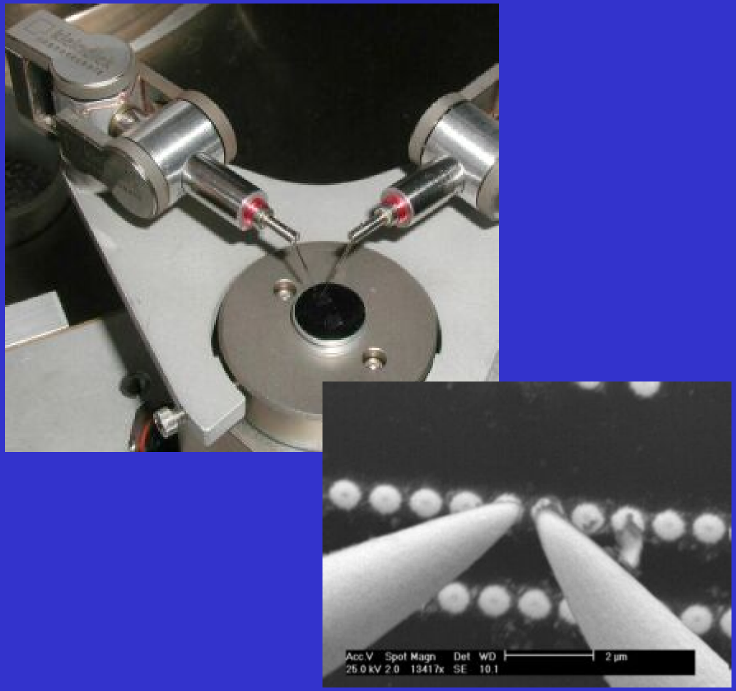

Sample preparation

1。Cross-section for failure analysis and design assistance

2。TEM sample preparation

- Cross-section of an integrated circuit

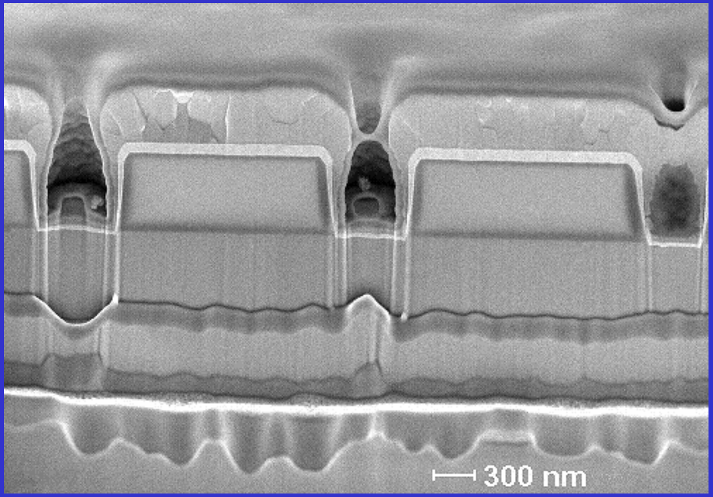

- TEM sample preparation

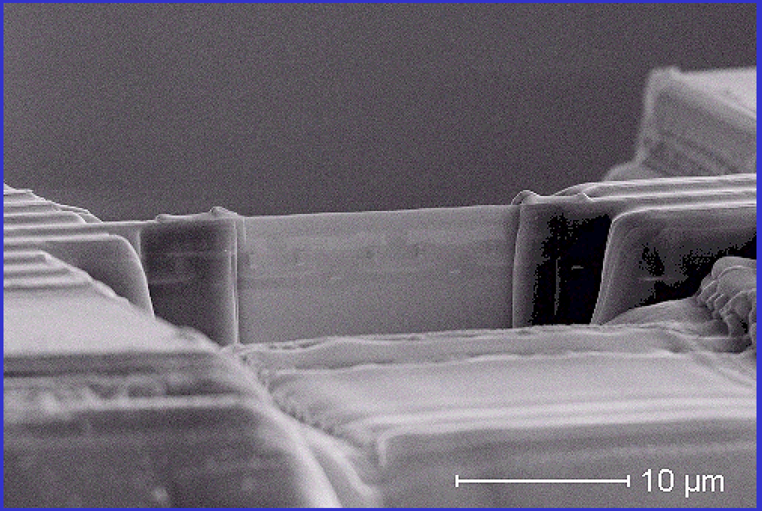

Device Modification

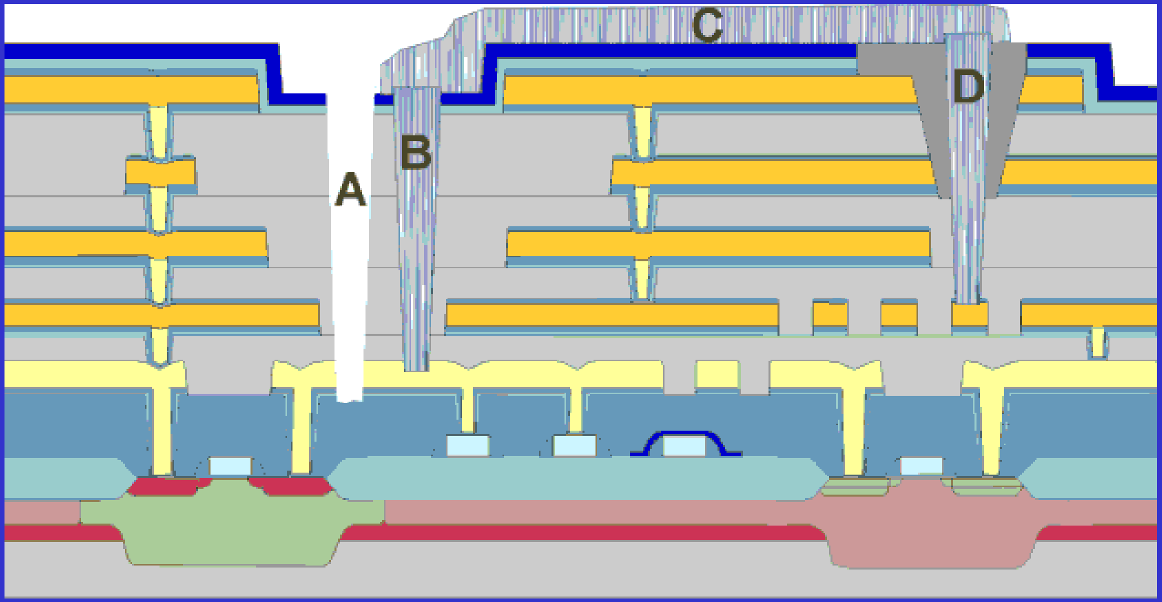

A: FIB cut to metal 1. B: FIB via to metal 1.

C: FIB strap joining vias. D: FIB via to metal 2.

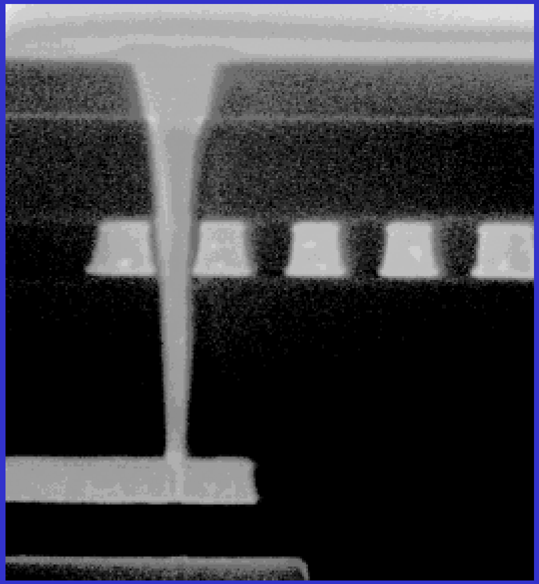

Deep Probe Point Filled with Conductive Material

Other Facilities

Sputtering System

CVD

Reactive Ion Etching

Surface Profile

Wire Bounder

Probe Station

SEM

FIB在纳米制造方面的应用

The processes for fabricating Pt nanopillar arrays

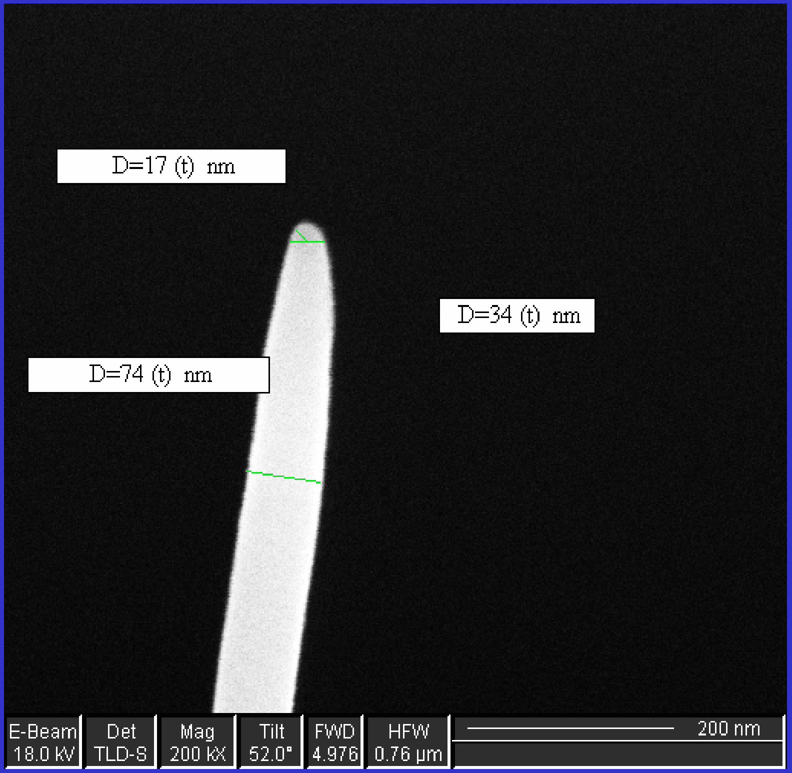

Aspect ratio: 50:1
Tip curve radius: 17 nm

After optimization of Pt deposition and milling parameters, the Pt nanopillar arrays with height of 8.5 um and tip radius about 17 nm were obtained.

FE I-V properties of Pt pillars deposited at different accelerating voltages

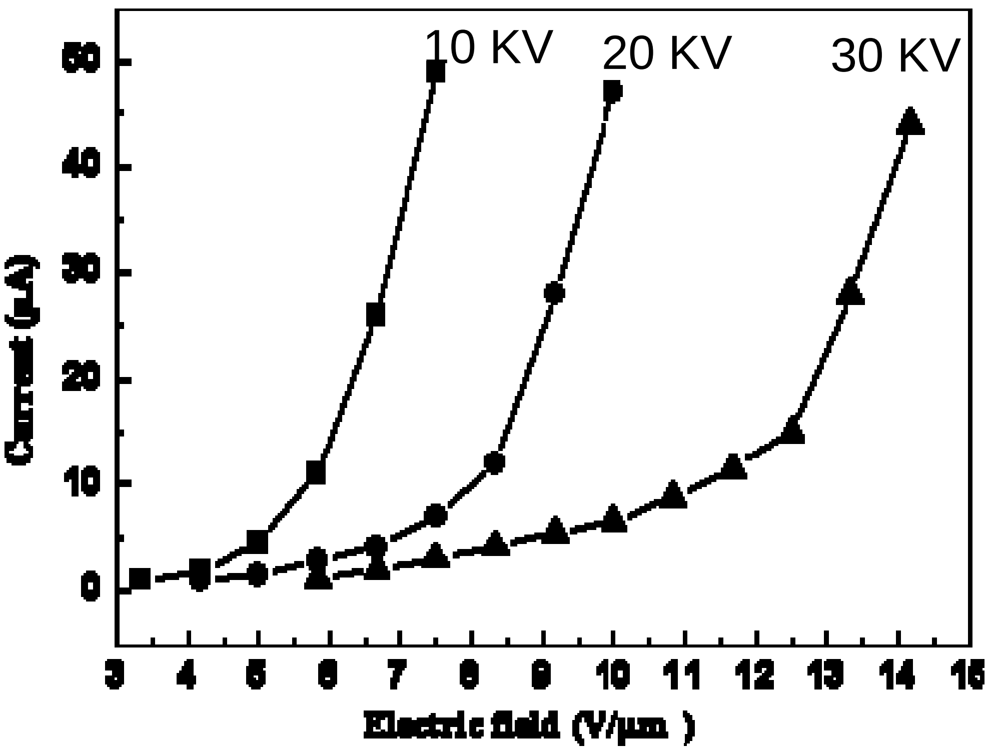

三维结构制造

(a) Fabrication process for three-dimensional nanostructure by FIB CVD
(b) Microbeakers with 1,0 and 1.5 um diameter, and 1,0 um height
(c) Microwine glass with 2.75 um external diameter and 12 um height

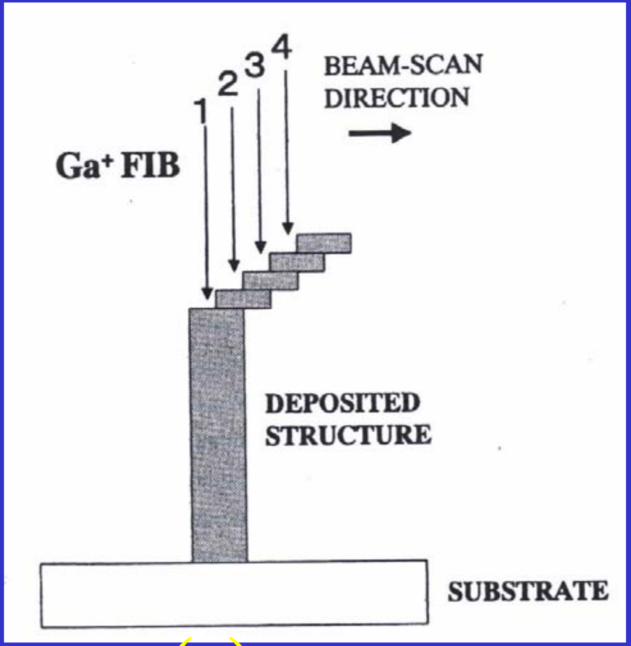

(a)

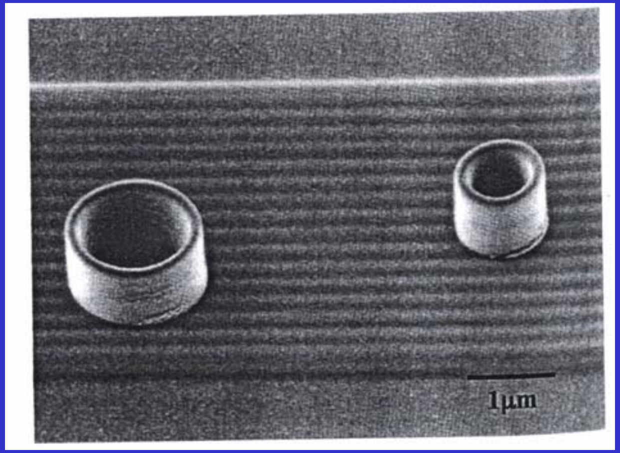

(b)

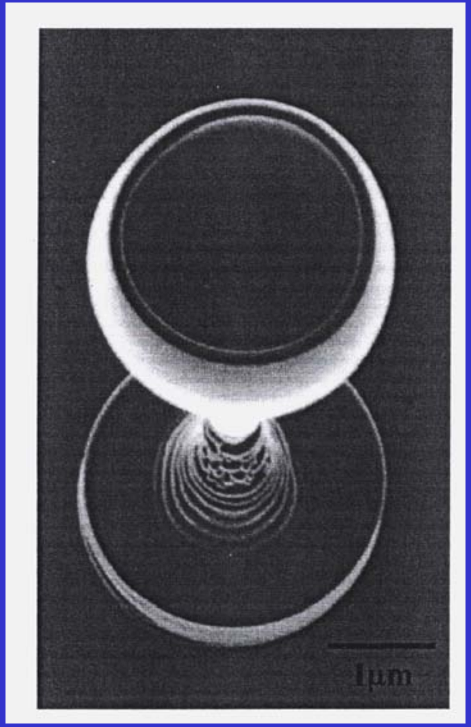

(c)

(a) Microcoil with 0.6um coil diameter, 0.7um coil pitch, and 0.08um linewidth

(b) Microbellows with 0.8um pitch, 0.1um thickness, 2.75 um external diameter, and 6.1um height

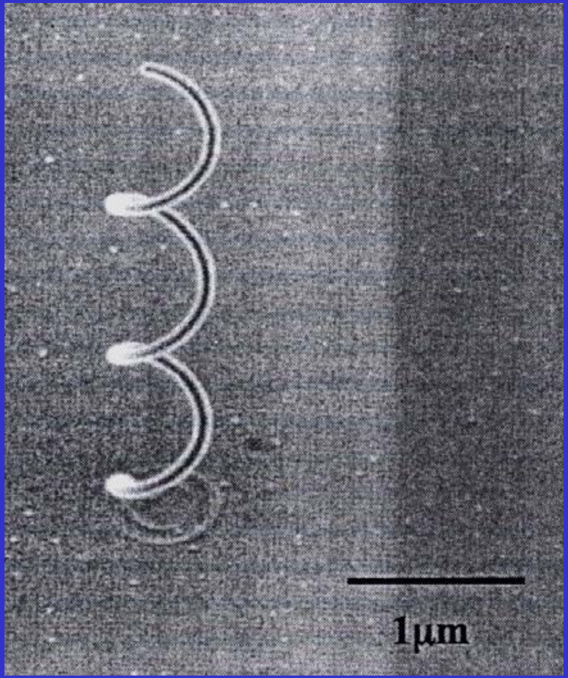

(a)

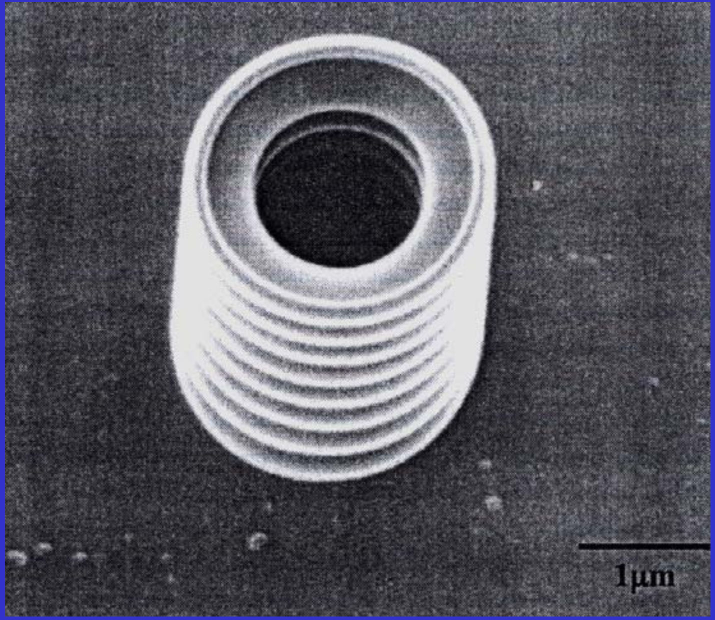

(b)

微纳米加工技术的应用

低维材料的输运性质、器件与电路

Quantum lines and dots

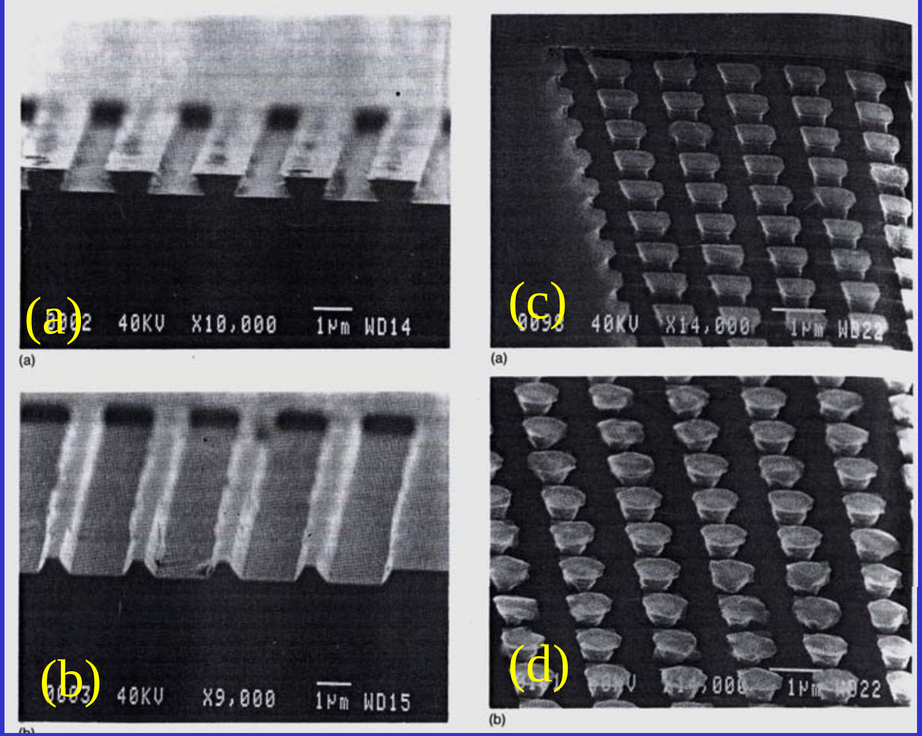

(a) Lines parallel to [110]: patterning width 1 um, period 2.25 um

(b) Lines parallel to [11/0]: patterning width 1 um, period 2.5 um. Note the etch pits on the upper surfacein (a)

(c) dots with exposed regions patterned at 0.5 um, period 1.2 um, etched for 1 min

(d) Dots with exposed regions patterned at 0.5 um, period 1.4 um, etched for 4 min. Note the incomplete etch down to the GaAs stop layerin (c). Some electron-transparaent flakes of GaAs cap layer and QW are visiblein (d)

1.55μm光致发光特性的InAs/InP 量子点阵列

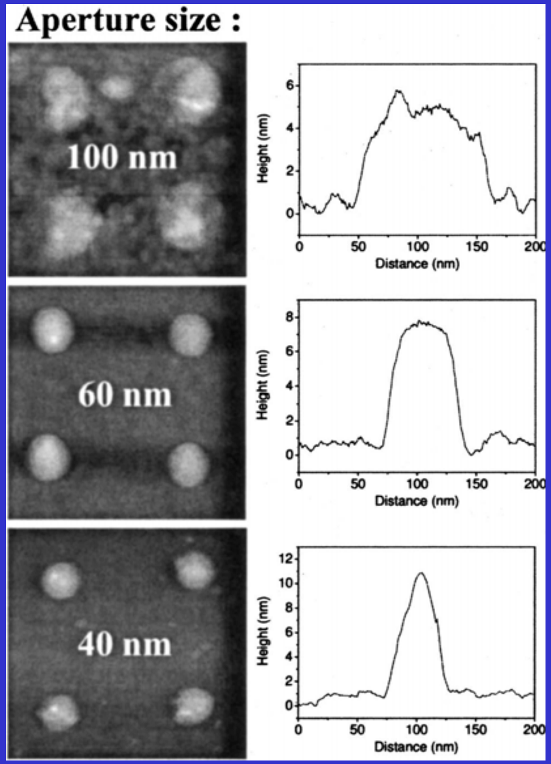

- 控制纳米结构材料的精确度已成为一种非常有挑战性的工作。人们利用分子束外延或化学束外延方法制作了InAs/InP 量子点，但这种方法制作的量子点沿［1－1 0］晶向会有一定的拉长。
- 将电子束曝光及金属有机气相外延方法相结合，制作出了直径为40-100nm的InAs/InP 量子点阵列。
- 发现该方法可以很好的控制量子点的尺寸及密度，且所得量子点的尺寸及高度波动很小，并在电信通信波段1.55μm波长处有高效的光致发光效应。

J. M. Benoit

Appl. Phys. Lett. 88（2006）041113

多壁碳纳米管的多通道弹道输运特性

双探针SEM原位测量系统的建立

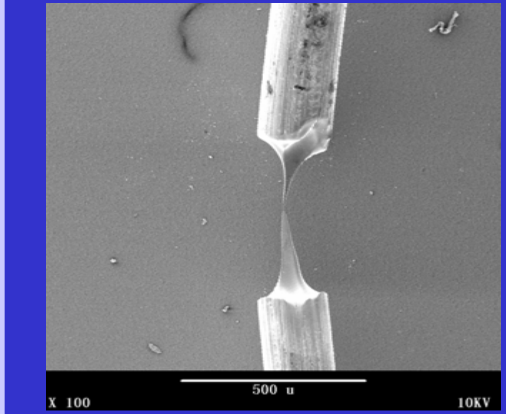

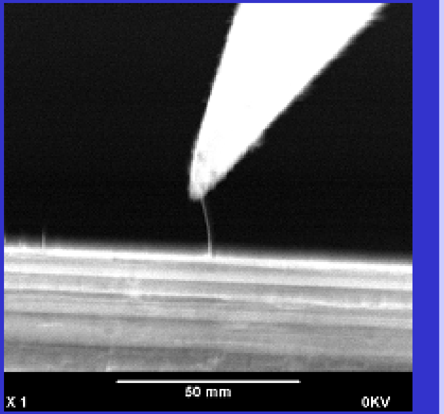

专利:2003201002228　　2002133050.6

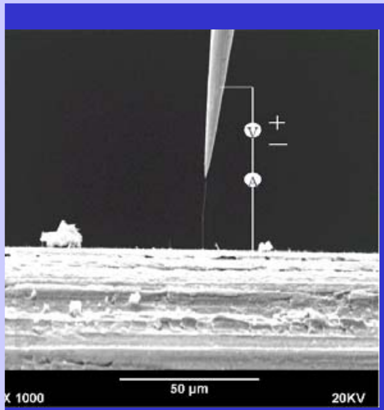

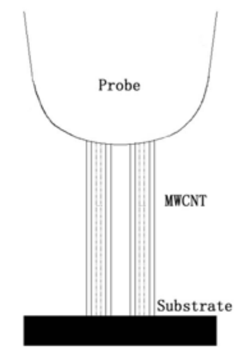

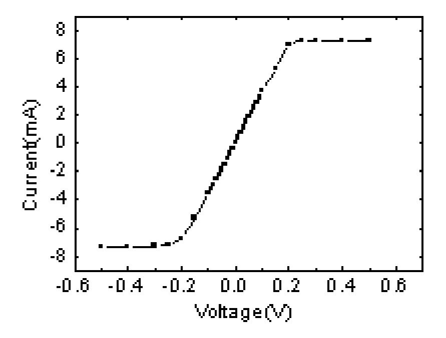

多层管壁参与
大直径 (100nm)
室温测量

$$f_i = \frac{1}{e^{\frac{|E^i_{occ} - E_F|}{k_B T}} + 1}$$

$$N = \sum_j^{N_{wall}} \sum_i^{N^j_{occ}} f_{ij} = \sum_j^{N_{wall}} \sum_i^{N^j_{occ}} \frac{1}{e^{\frac{|E_{occ} - E_F|}{k_B T}} + 1}$$

高功率器件
电路互连线

多层管壁的接触 → 大电流承载能力 7.25mA （$460G_0$） → 多通道弹道输运 （理论$455G_0$）

Physical Review Letters 95（2005）086601

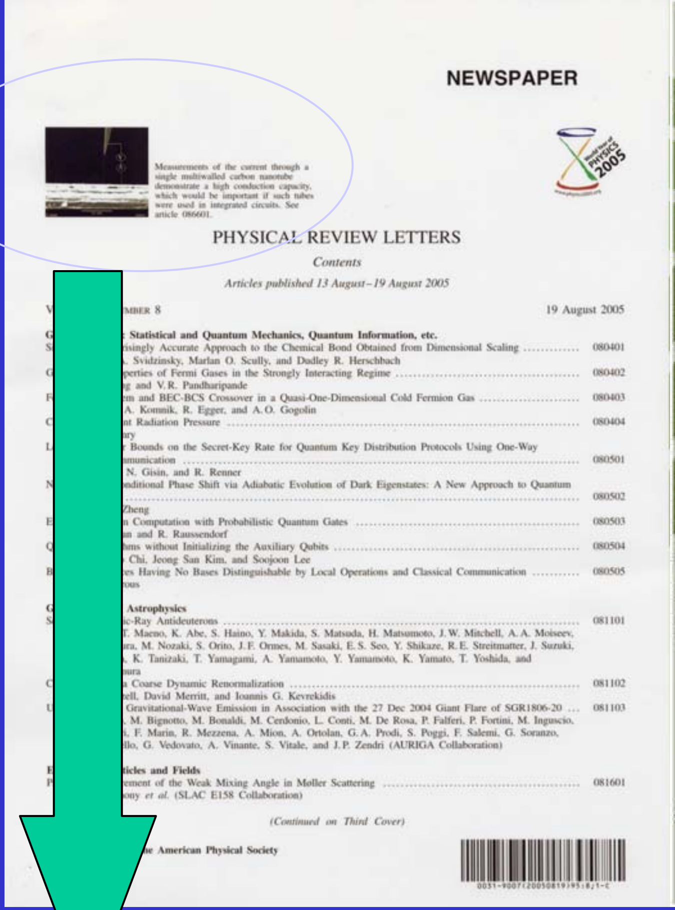

NEWSPAPER

Measurements of the current through a single multiwalled carbon nanotube demonstrate a high conduction capacity, which would be important if such tubes were used in integrated circuits. See article 086601.

PHYSICAL REVIEW LETTERS

Contents

Articles published 13 August–19 August 2005

V MBER 8 19 August 2005

(Continued on Third Cover)

e American Physical Society

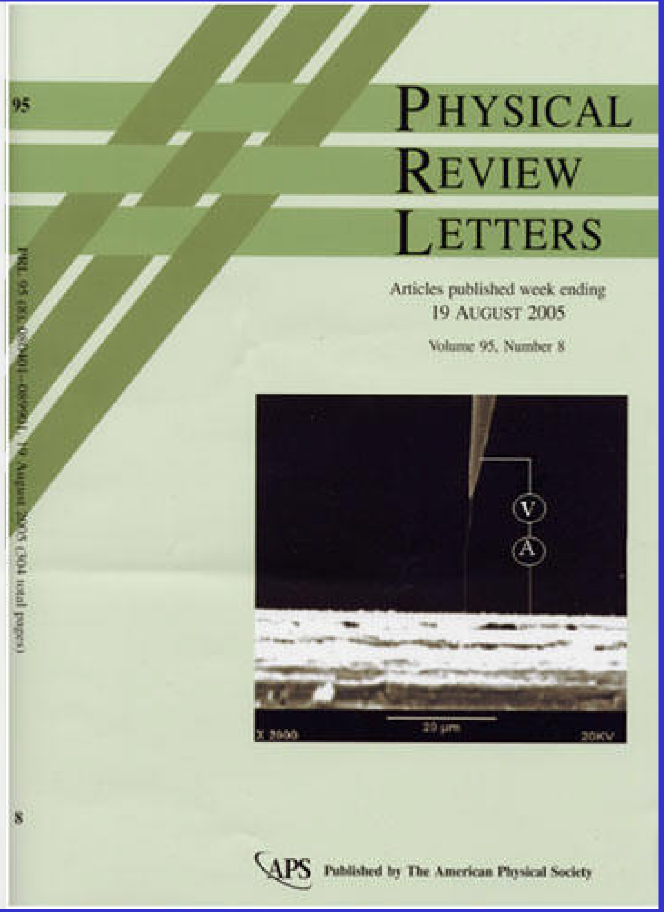

95

PRL 95 (8) 080401–089901 19 August 2005 (304 total pages)

8

PHYSICAL REVIEW LETTERS

Articles published week ending
19 AUGUST 2005

Volume 95, Number 8

APS Published by The American Physical Society

“单根多壁碳纳米管的电流测量证明了其高导电能力，在集成电路方面具有重要应用价值。”

Three-terminal carbon nanotube junctions: Current-voltage characteristics

L. Liu et al. Phys. Rev. B 71 （2005） 155424

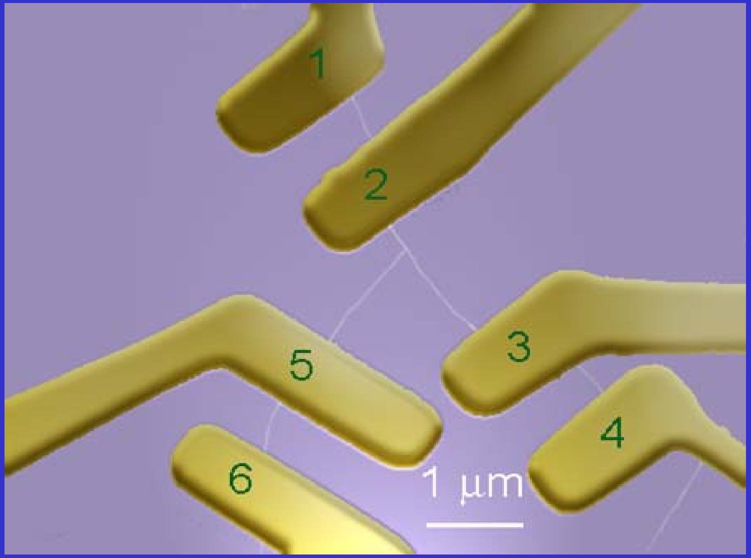

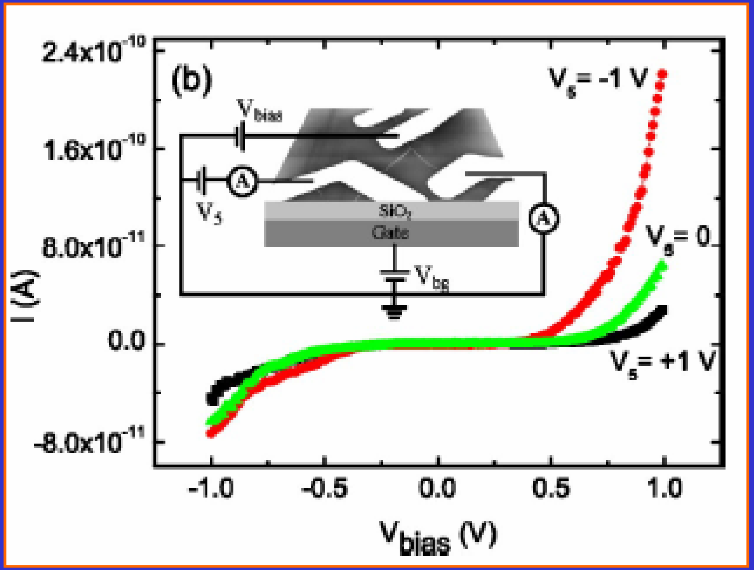

The current in the first nanotube (connected to electrodes 2 and 3) can be influenced by the voltage applied to the second nanotube (connected to electrode 5) which acts as a local gate electrode.

亚2nm碳纳米管内的物质输运特性

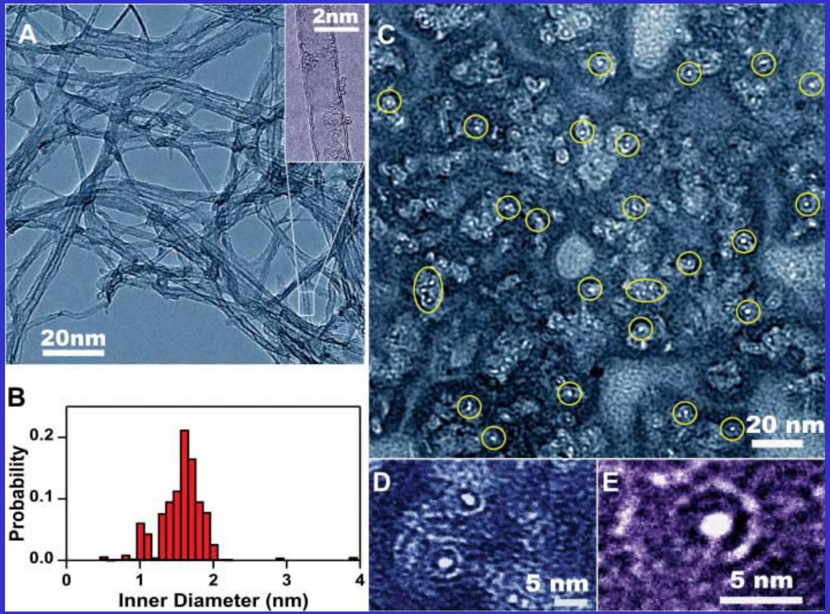

Jason K.Holt

Science 312（2006）1034

- 直径在纳米量级的碳纳米管，由于其拥有原子级的光滑内表面成为研究分子输运和纳流体的独特系统。
- 将电子束曝光、化学气相沉积及刻蚀的方法相结合制备出了能够进行物质输运测量的以双层碳纳米管为主的系统。
- 并利用该系统对多种气体及水在其中的输运进行了研究，研究发现该系统对气体的传输速度比努森模型预测的值高一个数量级，水的传输速率则比分子动力学模拟结果高三个数量级。

高速集成纳米线电路

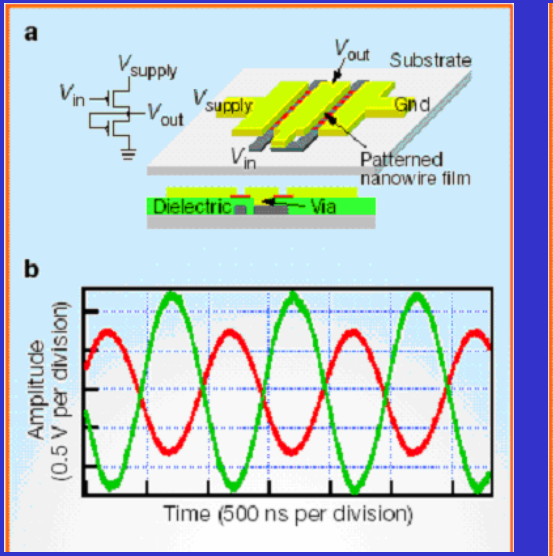

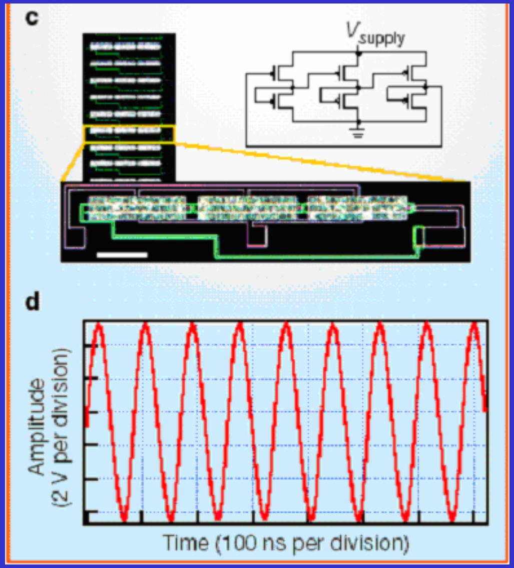

Robin S. Friedman

Nature 434 (2005) 1085

- 在玻璃或塑料衬底上制作电子线路由于重量轻、弹性好、成本低，将来可能会用于制作计算器件。
- 采用标准的光刻技术，通过低温平面工艺在玻璃衬底上将高性能的多纳米线晶体管集成为逻辑反相器和环形震荡器，反相器由两个纳米线薄膜晶体管组成，环形震荡器由三个反相器串联而成。
- 制作的环形震荡器的震荡频率高于硅衬底上制作的器件，达10 MHz以上；相应的延迟时间远小于有机半导体和非晶硅器件，仅为14 ns。

单个分子对的电导测量

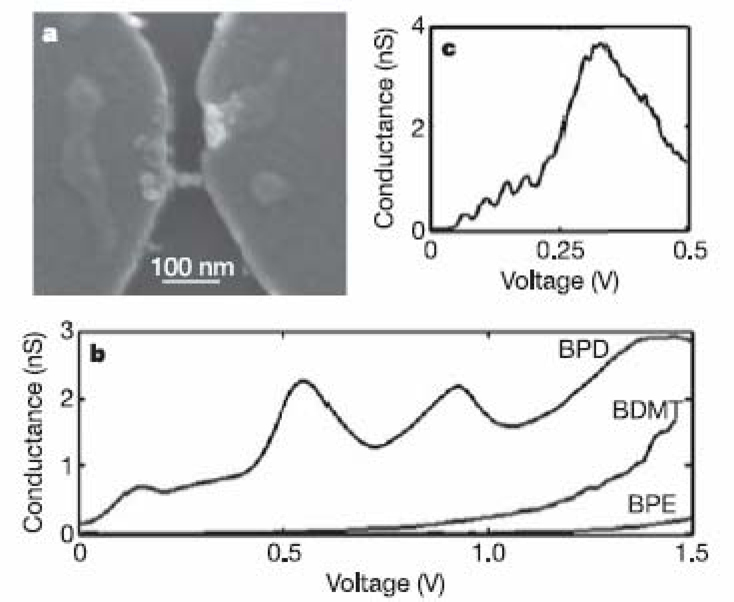

Tali Dadosh

NATURE677（2005）**436**

- 由硫醇基（SH—）键合而形成的有机分子是良好的分子导体，在单分子器件的制备中有巨大潜力。
- 采用了一种测量单个有机分子导电特性的新方法，用以研究在共轭分子中一些局域基团对电导的影响。
- 该方法首先合成二聚体（即用BDP，BPE, BDMT有机分子来连接两个金胶体颗粒），然后采用静电捕获的方法将其捕获在金电极上。二氧化硅衬底上金电极的制备采用了电子束直写（EBL）的方法。
- 相对于BPD而言，BPE中的氧和BDMT中的甲烷都能对分子电导造成抑制。

用导电分子连接单壁碳纳米管

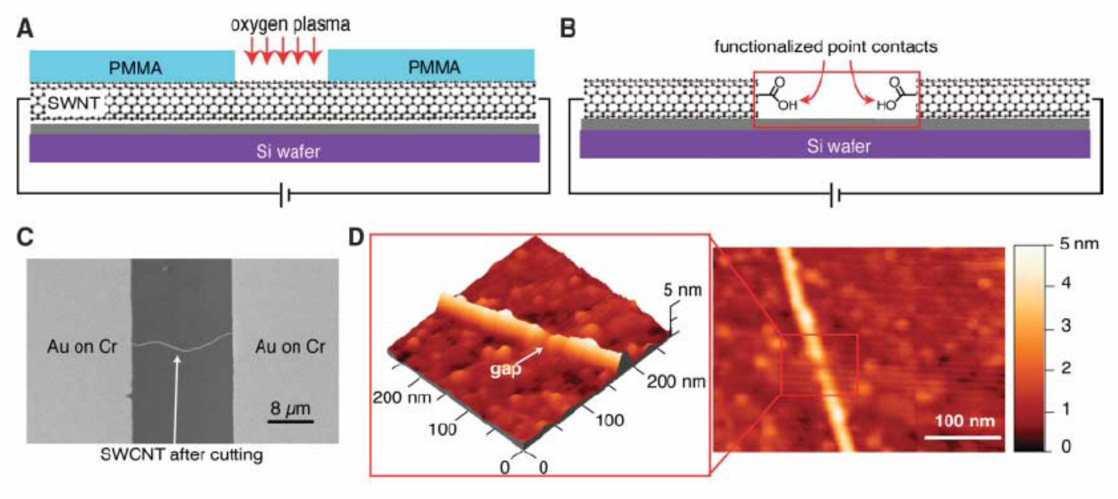

Xuefeng Guo

Science
311 (2006) 356

- 分子与金属电极之间的结合情况不明了是分子电子学面临的最大挑战之一。
- 采用电子束曝光和氧等离子体刻蚀单壁碳纳米管形成间隔小于10 nm的、两侧由羧酸终止的裂缝，将分子通过共价键连接在单壁碳纳米管的裂缝间，形成了非常牢固的接触。
- 这种方法可用于多种分子的电学性质测量。另外，还发现这样的单分子桥的电导会随着pH值的变化而转变。

二维石墨片中的量子霍尔效应

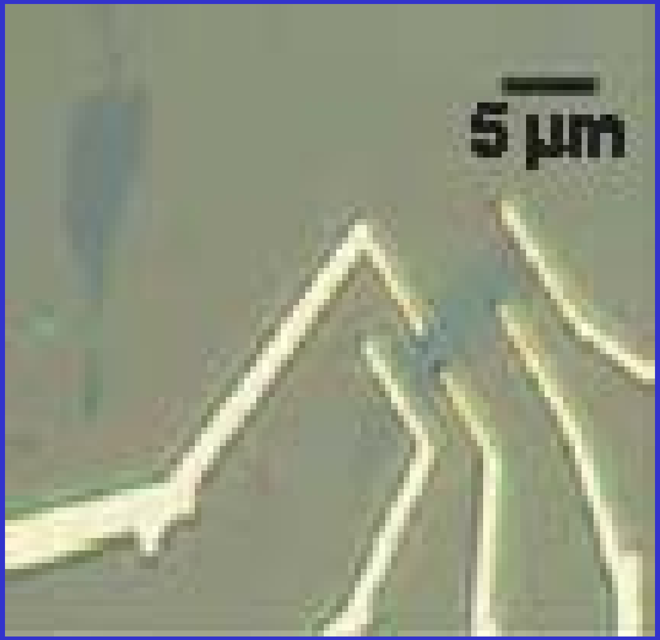

Yuanbo Zhang

Nature 438 (2005) 201

- 二维石墨片是现实中的理想二维系统。理论早已预言了特殊的半整数量子霍尔效应,以及由二维石墨层能带结构的异常拓扑结构导致的量子波函数非零Berry相的存在。
- 利用微机械提取加工工艺得到了高迁移率的单层石墨层，利用电子束光刻制备了二维石墨层金属电极，进行了磁致输运的实验研究。
- 观察到了电子以及空穴的半整数量子霍尔效应，同时磁致震荡验证了这些实验与Berry相之间的联系。

磁学方面的应用

- **MTJ**
- 自旋霍尔效应
- 畴壁

The test structure of ferroelectric properties

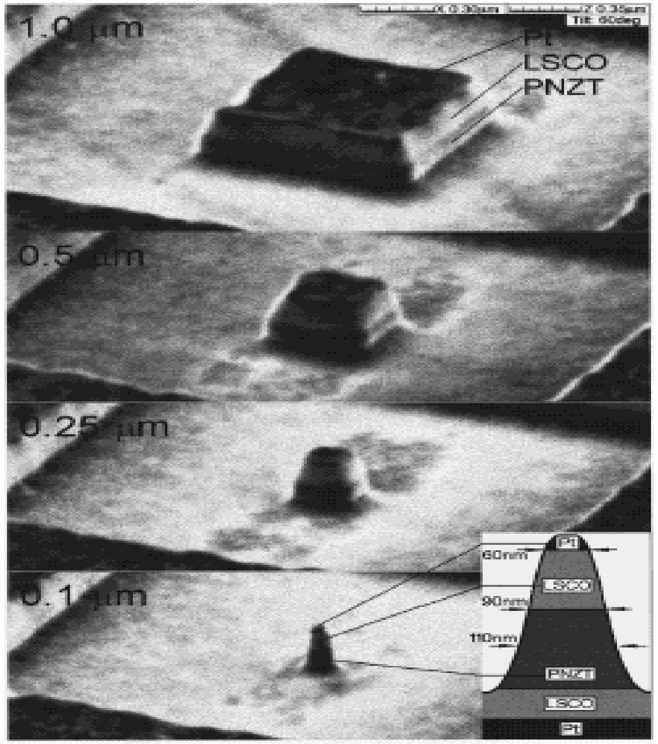

FIG. 1. Scanning ion-beam images of the test structures fabricated by focused ion-beam milling in the size range from 1 μm×1 μm to 0.1 μm×0.1 μm. The contrast from the various layers in the heterostructure is also indicated. The inset is a schematic of the shape and dimensions of the 0.1 μm test structure.

FIB milling in the size range from 1um^2 to 400 nm^2

单磁畴壁的谐振特性和质量的测定

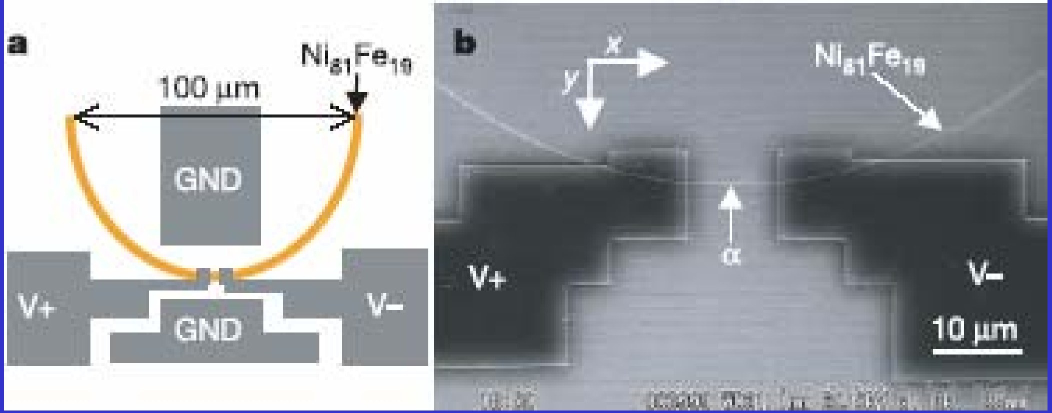

J. Saitoh

Nature 432 (2004)203

- 磁畴壁的质量可以通过磁共振效应直接测得，它决定器件的最终工作速度，并且对高密度磁存储器的发展特别有益。
- 在热氧化的硅片上，利用电子束曝光技术制作了一个由Ni81Fe19纳米线构成的半园环结构及两个测量电极。
- 使用高频交流电流直接观察到了铁磁纳米线中单个畴壁的动力学特征，从而准确测定了一个畴壁的质量。
- 结果表明单磁畴壁具有6.6×10-23 kg的有限质量。

自旋电流引起的磁畴壁形状变化

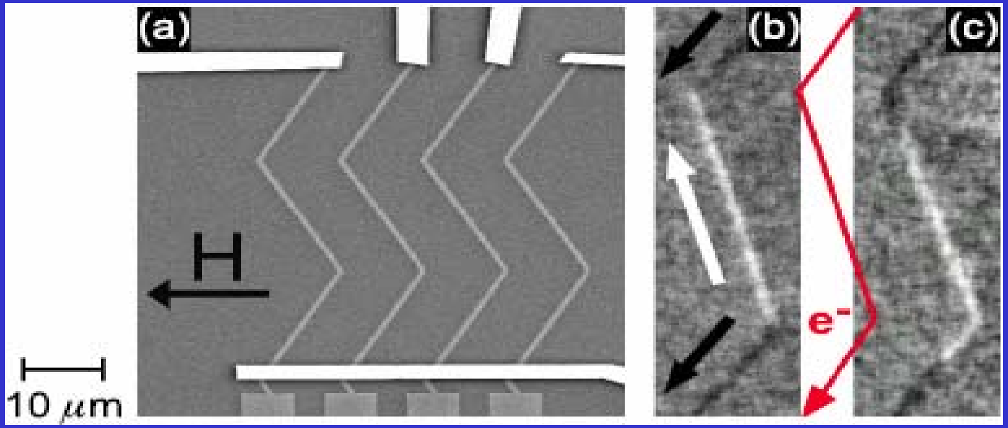

Kläui
Physical Review Letters
95（2005）026601

- 控制纳米结构中的磁化方向是自旋电子器件应用的关键，利用自旋迁移效应，注入自旋电流可以改变磁畴畴壁的位置，从而改变纳米结构中的磁化状况。
- 在硅衬底上，利用电子束光刻技术制作了一系列不同宽度的Ni80Fe20纳米线，宽度范围从100nm到500nm，并利用自旋极化扫描电子显微镜直接观察到在脉冲电流作用下磁畴畴壁沿着纳米线移动，导致畴壁形状的变化。
- 使用这一结构，畴壁在宽度500nm、厚度10nm的Ni80Fe20纳米线中沿着电流方向以平均0.3m/s的速率移动，并且速率随着脉冲个数的增加而衰减。

Submicrometer Ferromagnetic NOT Gate and Shift Register

D. Allwood, Science, 296(2002)2003

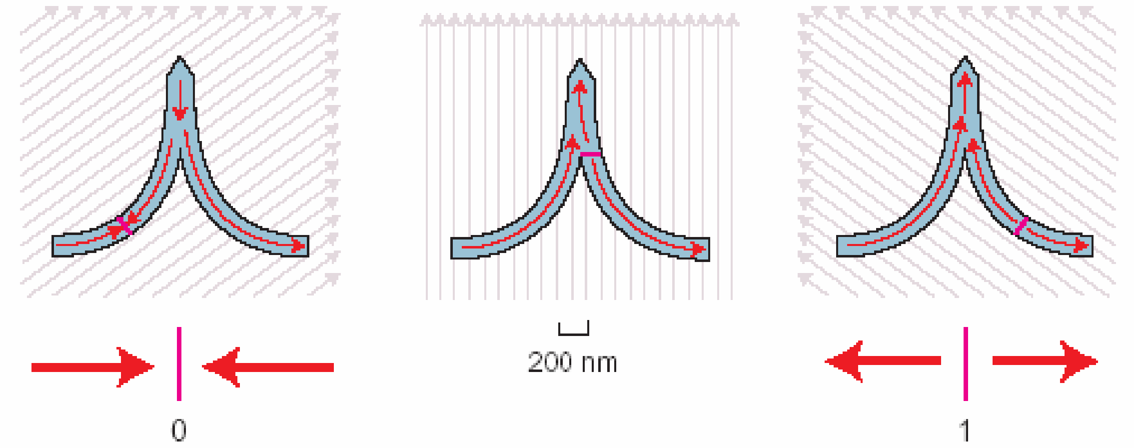

A rotating magnetic field changes the value of a bit by moving and then flipping the boundary between regions of magnetized wire.

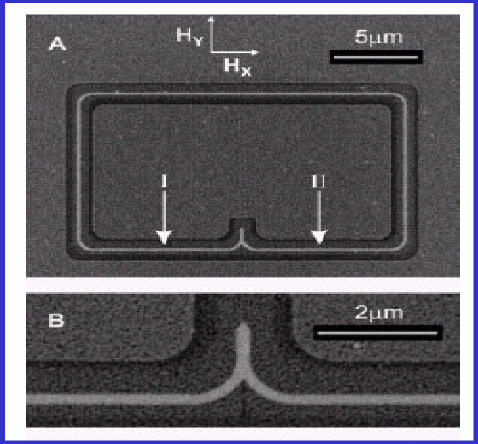

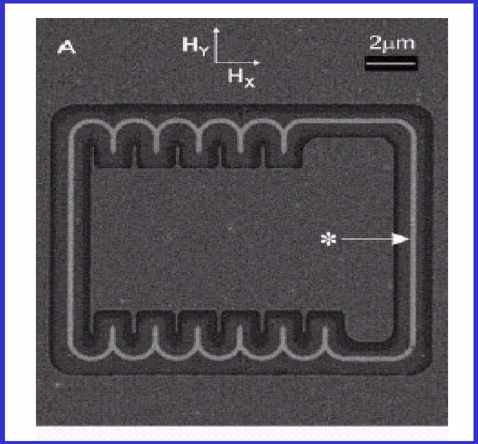

光学方面的应用

- 光子晶体
- 左手材料（**metamaterials)**
- **Plasmon**
- 全光开关

光子晶体

两种或两种以上介质的周期性排列组成的一种人造晶体。由于介电参量的周期调制，一定频率的电磁波在光子晶体特定方向上被散射，不能透过，形成光子能带禁带。

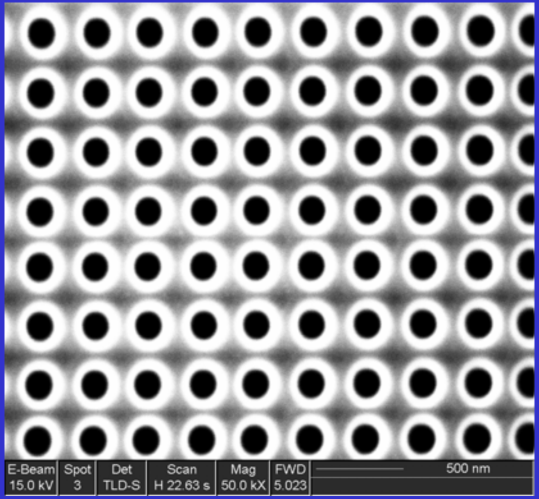

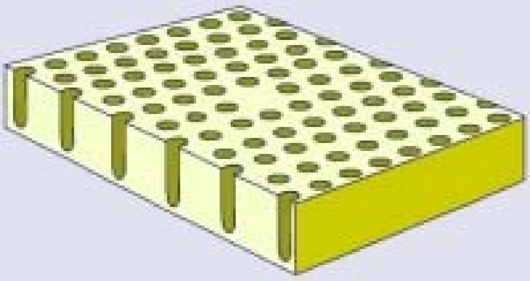

点缺陷

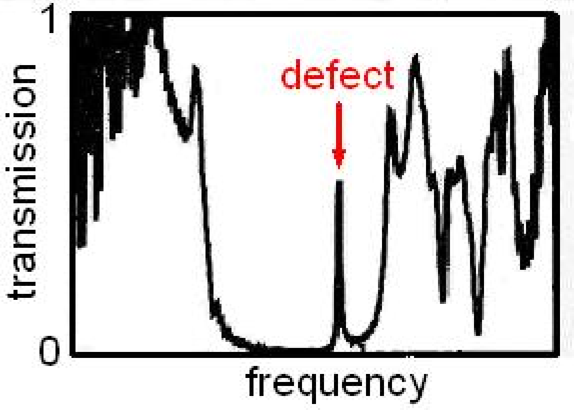

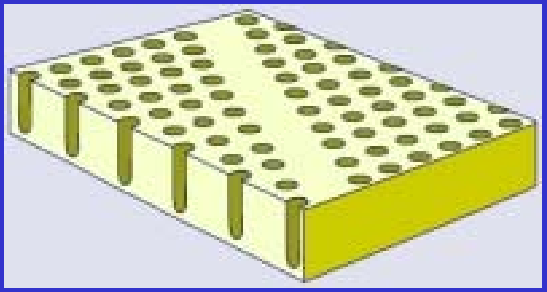

线缺陷

科学意义：

建立了光子的能带理论，打开了控制光的传播及光与物质相互作用的新领域—凝聚态物理和光学的新交叉领域。

创造了一种人工设计的新材料---光子半导体。

应用领域：

无阈值激光器、天线、光波导、微腔、光分复用器、选频器

光子器件、反射镜、光开关、光放大

集成光路

具有光子晶体结构的蝴蝶翅膀

Butterfly Scales as Living Photonic Crystals

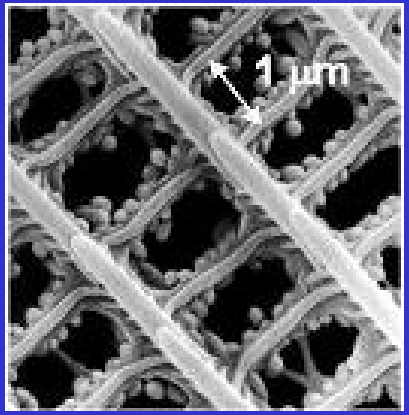

短间隔直接耦合双通道滤波器

port1 port2

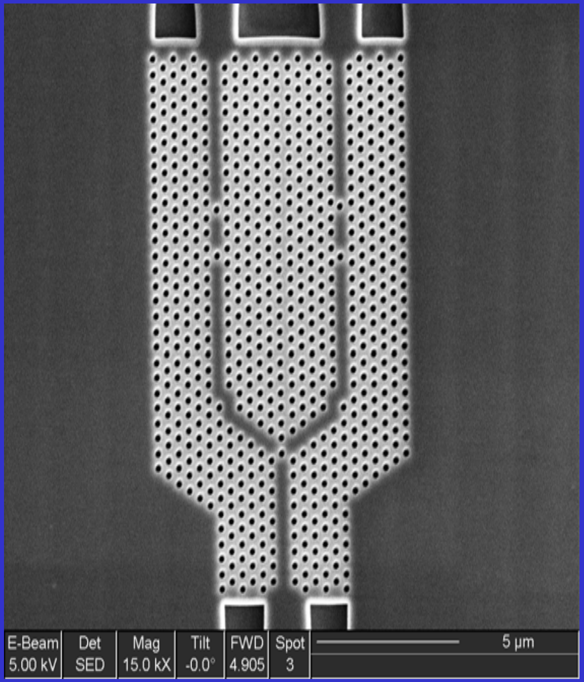

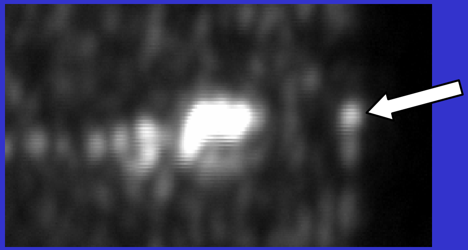

1572nm

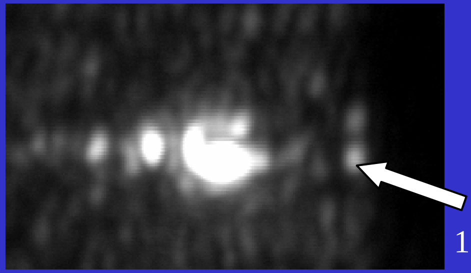

1567nm

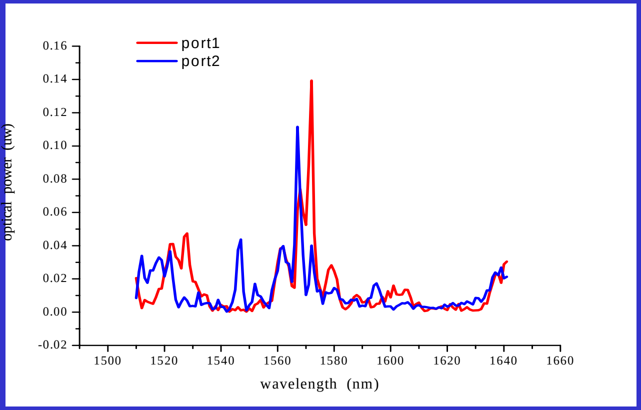

测量结果显示,两通道输出的峰值波长相差仅**5nm**

Left-hand materials (LHM)

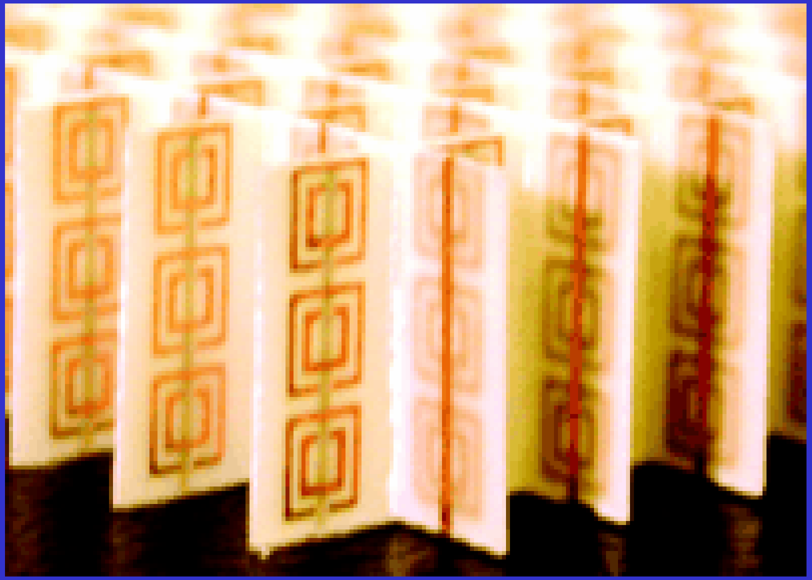

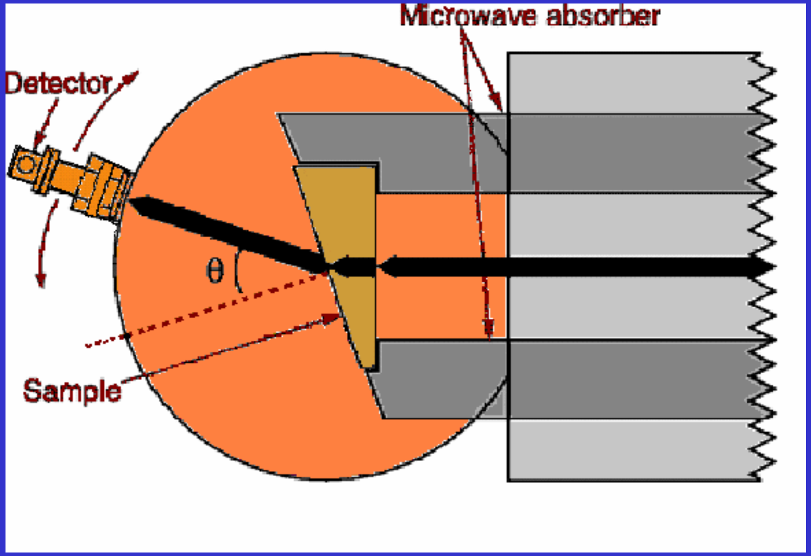

D. R. Smith
Science **292**(2001) 77

逆**Snell**定律及负折射
逆**Doppler**定律
逆**Cerenkov**辐射

波导、滤波器和高指向性天线等

异向性介质在100 THz的磁响应

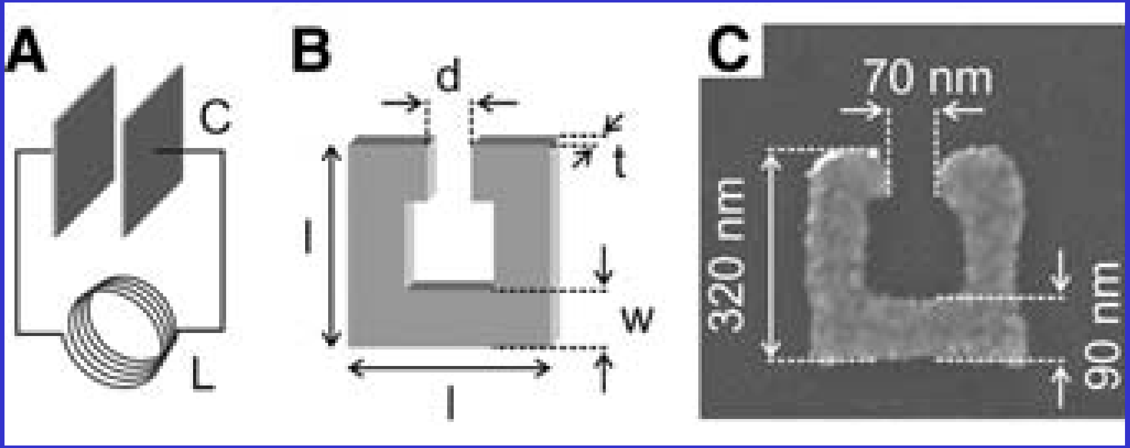

Stefan Linden

Science
306 (2004)1351

- 在太拉赫兹及更高频率实现磁共振响应对太拉赫兹光学和太拉赫兹电磁波的应用有非常特别的重要性。异向性介质（包括左手材料和开口谐振器环）能够在天然磁性材料没有磁响应的频率实现磁共振响应，从而使负折射率的实现成为可能。
- 利用电子束光刻和金属薄膜蒸镀制作的LC共振环，采用不同极化方向的红外光对这种微结构进行垂直照射，证实了这种结构在1 THz具有磁响应。

左手材料（THz、红外、可见）

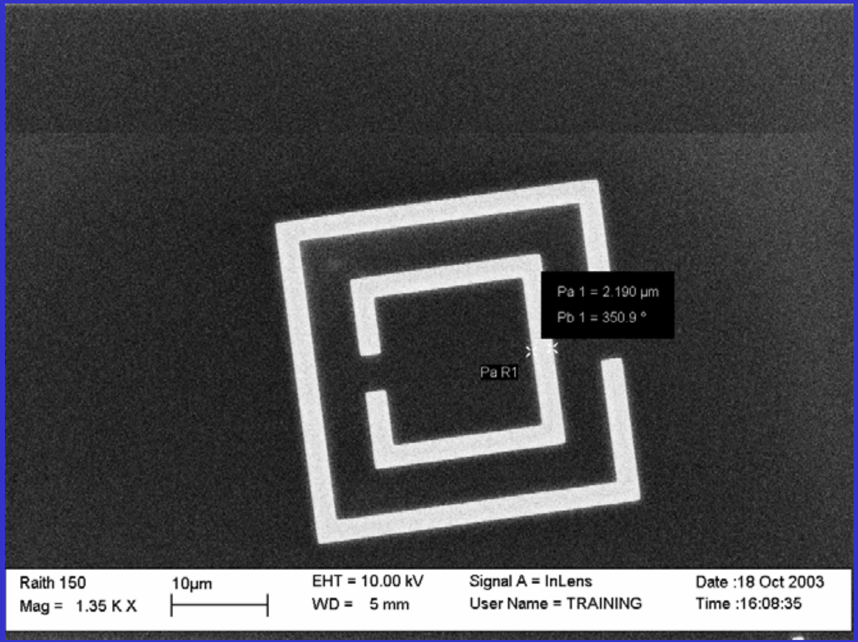

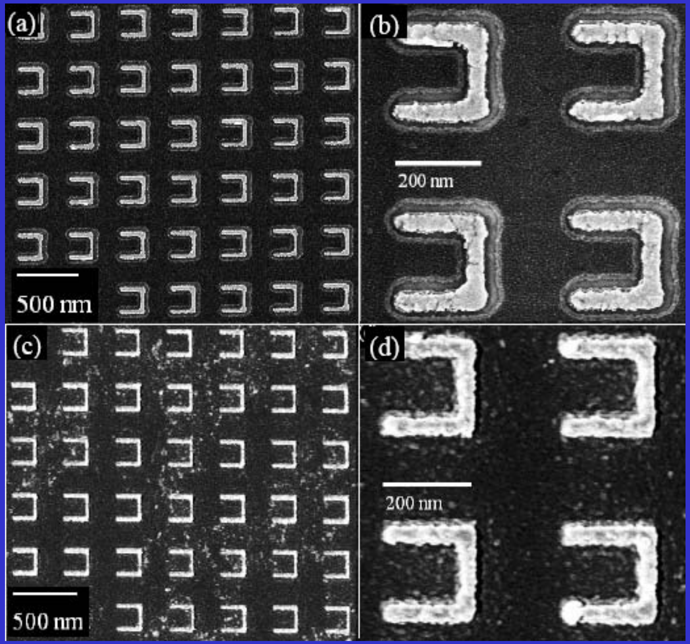

THz左手材料：生物学、安检、远程传感器、生物分子识别、新型雷达、全天候导航设备、远距离发现衣物内隐藏武器的探测仪器、检查配件质量的检测设备的研制等。

红外左手材料: 高密度存储技术，近场显微镜和突破光学曝光极限的光学曝光技术.

Beaming Light from a Subwavelength Aperture

金属膜上
60nm园孔
100%透过
650nm的光

SCIENCE
2002 VOL 297

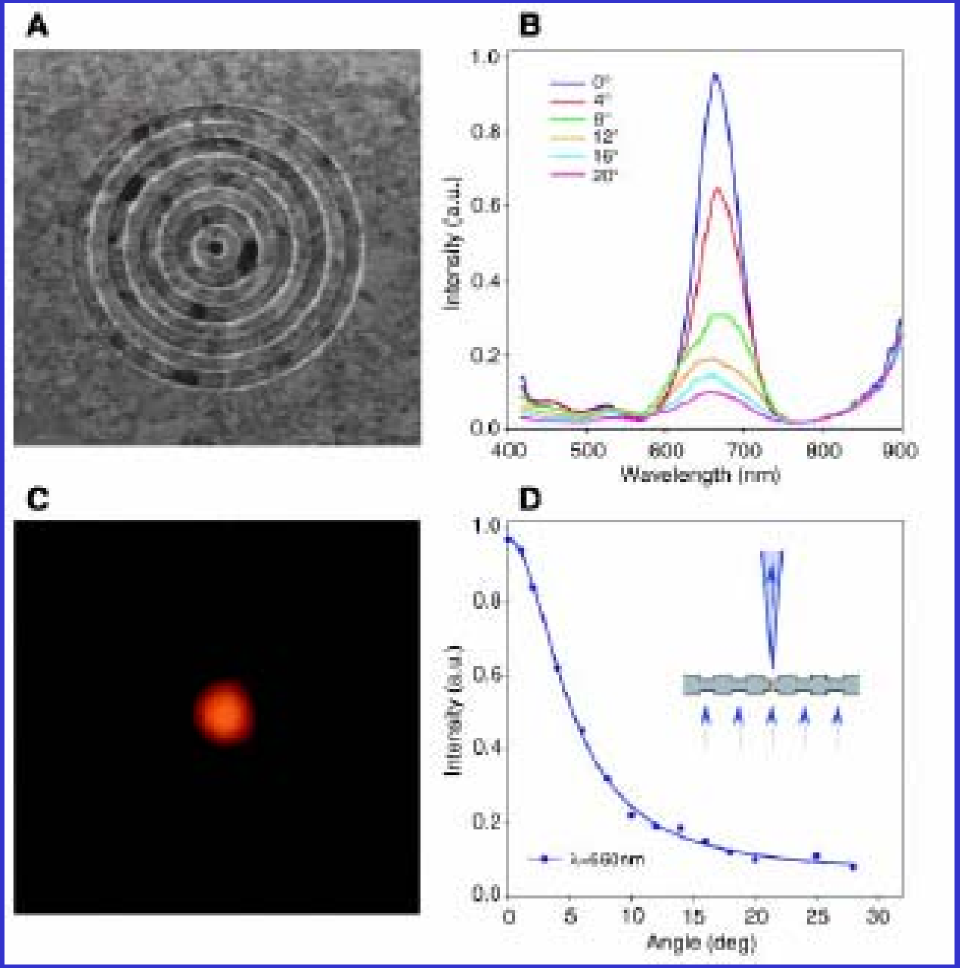

在硅芯片上制作全光开关

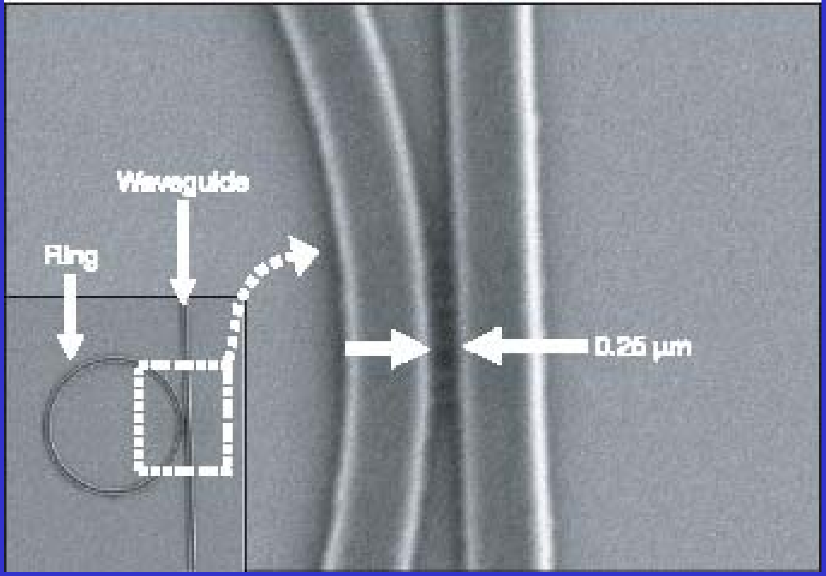

V. R. Almeida

Nature 431 (2005)1081

- 光子电路的制作是实现集成光学，并在通讯领域得到应用的关键，人们特别希望在廉价的、并在微电子领域应用广泛的硅芯片上实现光子电路。
- 在SOI衬底上，利用电子束光刻技术制作了一个环型共振器和波导，形成对光的限制结构。
- 实现了硅衬底上的快速全光开关与调制，使用这一结构，对25 pJ的光脉冲，在500 ps内可实现94%的传播调制。

ε

控制电磁波实现隐身

通过特定的介质空间的介电常数和磁导率分布，让电磁波绕过隐身目标后仍然恢复原来的传播路径，实现隐身效果。

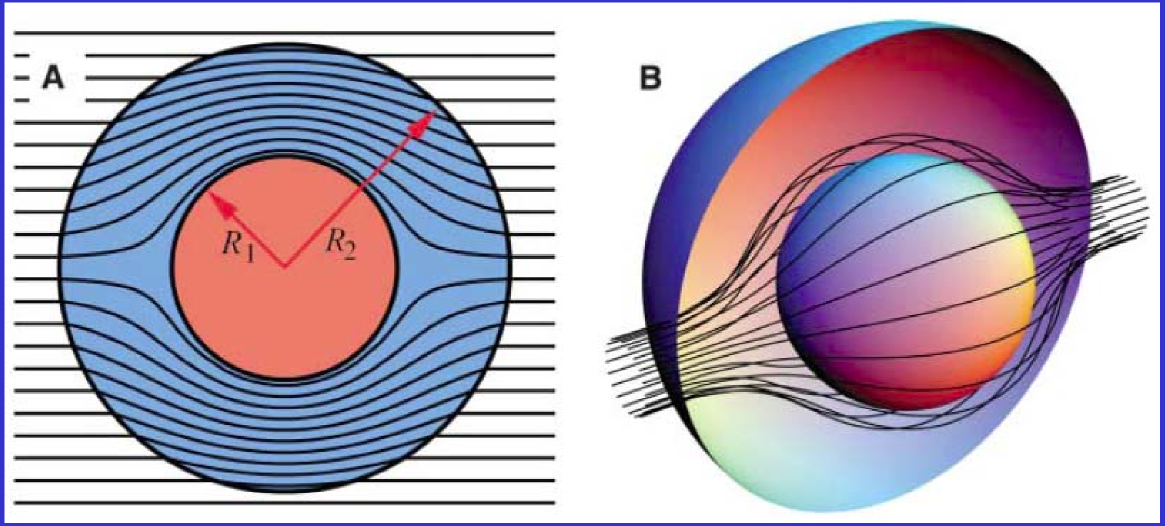

Science, 312 (2006)1780

ε

微波隐身材料

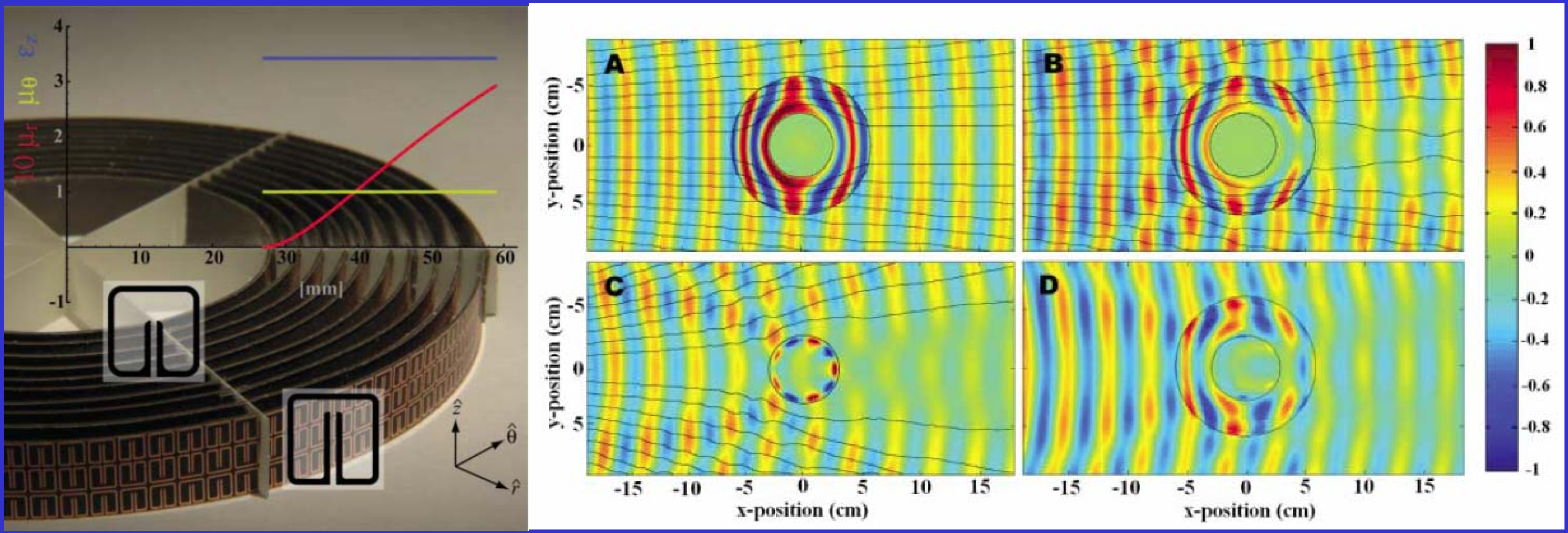

Science (2006)

ε

红外与可见波段的隐身

最近，伯克利大学的张翔等人，分别在近红外和可见光频域实现了具有负折射效应的左手材料，这意味着人类对高频电磁波传播的控制又上升到了一个新的高度，使得基于人工超材料的隐身技术研究在高频频域成为可能。

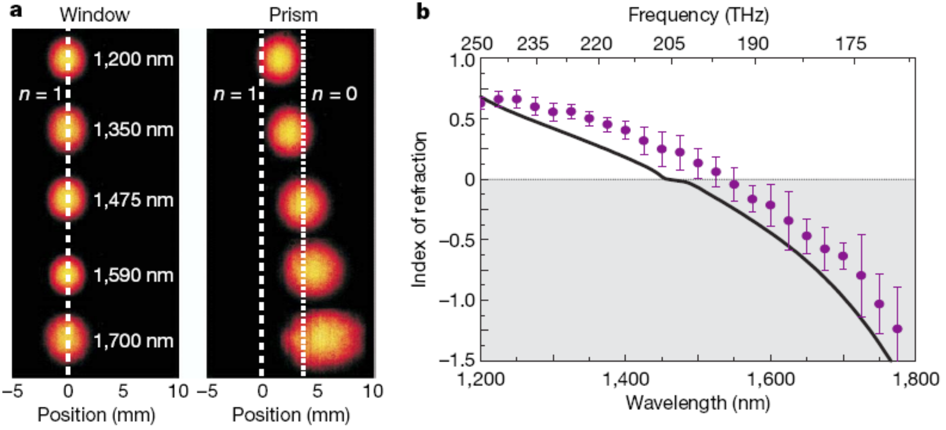

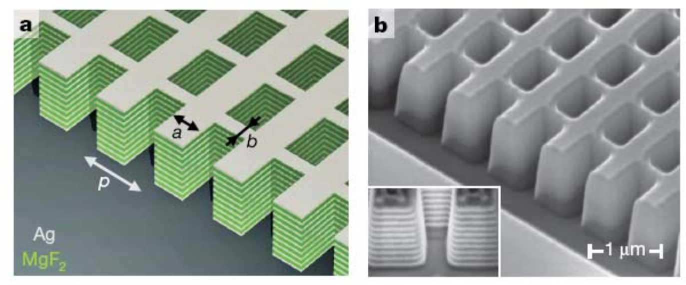

多层MgF_2/Ag渔网状的人工超材料，1475nm左右折射率变为0，当入射电磁波波长继续变大时转为负值，成功且直观地的实现了负折射效应。

Nature (2008)

DNA detectors

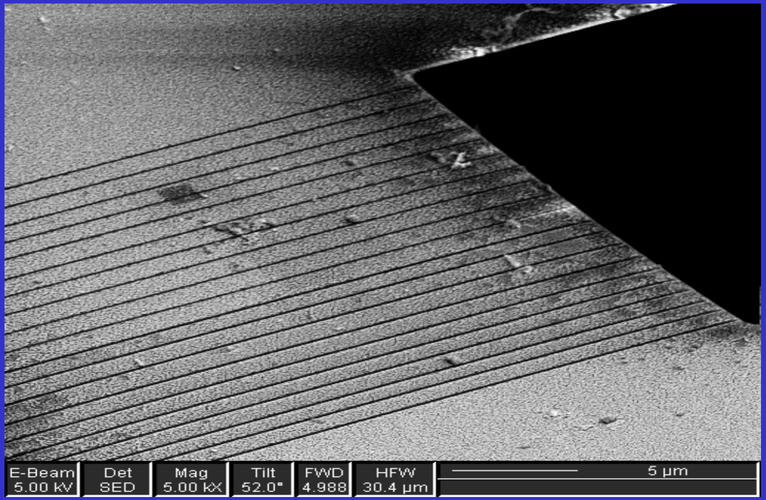

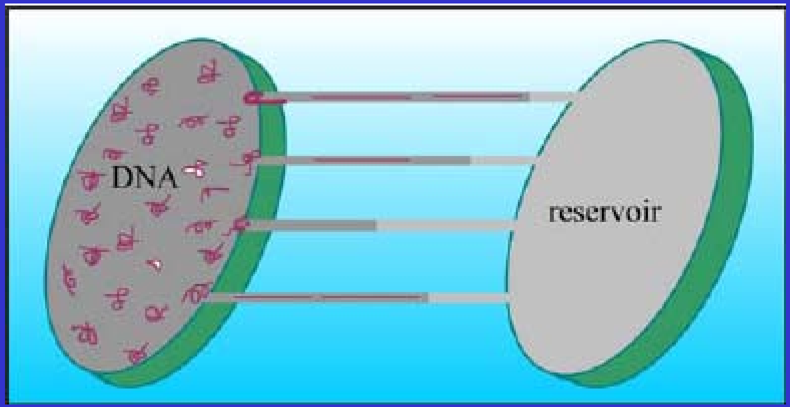

纳米通道中的单个DNA分子的静力学与动力学研究

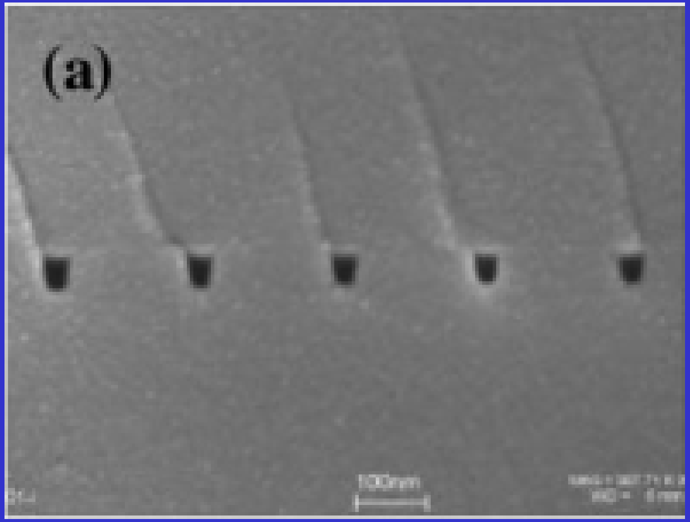

Walter Reisner

Physics Review Letters
94 (2005) 196101

- 生物芯片不仅可以对单个DNA进行逐个地检测和分离，而且还很有希望实现单分子量级的排列。
- 利用纳米压印直写和电子束曝光技术的结合在熔融石英衬底上制作出了不同宽度（30-400nm）的纳米通道，然后采用石英-石英键合的方法实现通道密封，进而对在密封通道中受限的单个DNA分子的静力学与动力学特性进行了研究。
- 结果表明能够实现“跨越”的纳米通道的临界尺度大致低于DNA持久长度的两倍，并得出了不同于经典的de Gennes理论的结论。

An all-metallic magnetic logic gate fabricated by Invar nanostructures

Introduction

Spin injection

- external magnetic field
- spin-polarized current

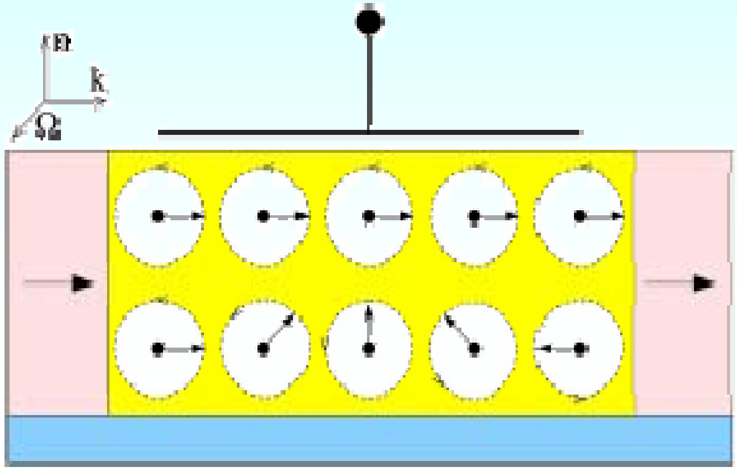

S. Datta and B. Das, Appl. Phys. Lett. 56,665(1990).

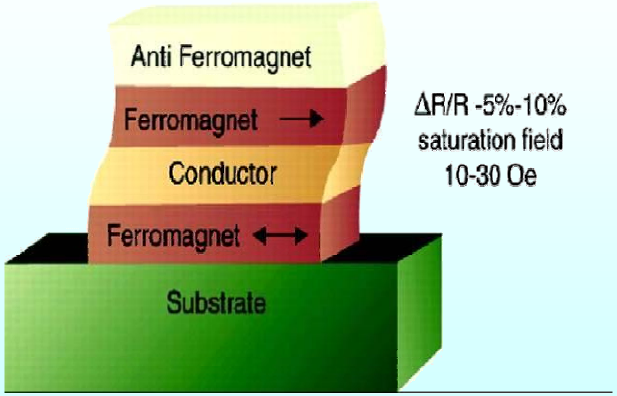

J. A. Katine, et al. Phys. Rev. Lett. 84,3149(2000).

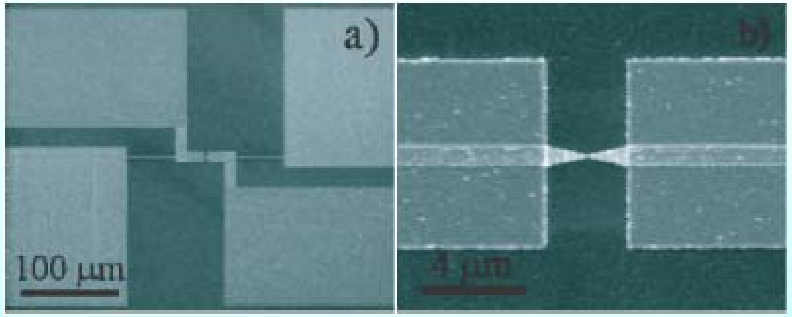

Y. B. Xu et al. Phys. Rev. Lett. 92, 127201(200

The nanoconstriction structures

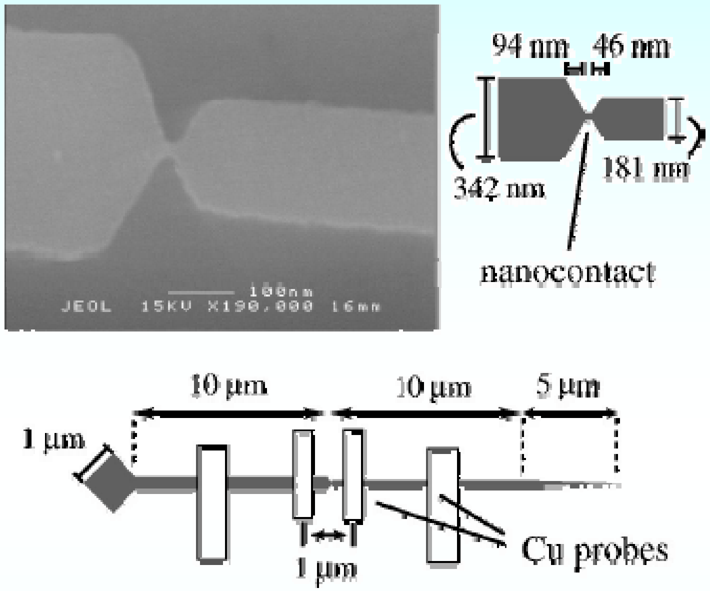

FIG. 1. Schematic illustration of the shape of a typical sample and the SEM image of the nanocontact between two wires. The narrowest square between two wires is defined as “nanocontact” in this article. The size of the nanocontact estimated from the SEM image was 15 × 13 nm^2.

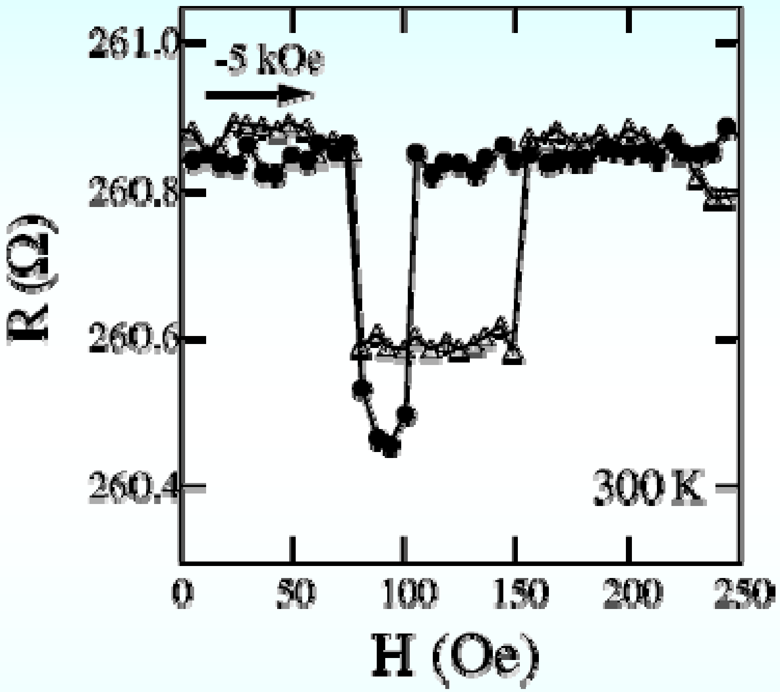

MR measurements. Micromagnetics simulation showed that a trapped DW at the nanocontact has an internal magnetic structure similar to a Néel wall inside the nanocontact. Two

K. Miyake et. JAP 97,014309(2003)

Domain wall motion in metal and semiconductor

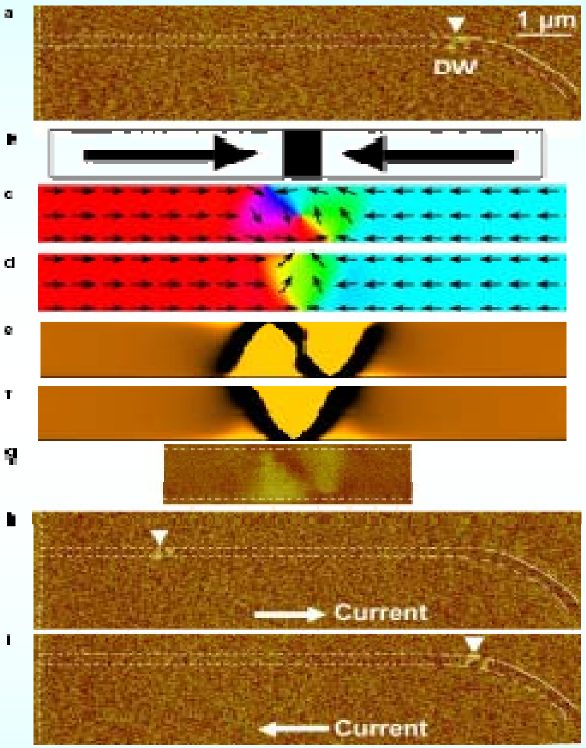

Yamagushi et al., Phys. Rev. Lett. (2004)

Yamanouchi et al. Nature 428(2004)539

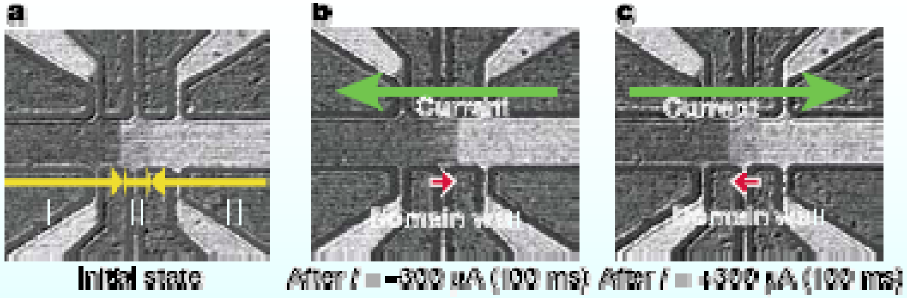

Initial state   After I = −300 µA (100 ms)   After I = +300 µA (100 ms)

Observation Domain wall motion in nanostructure

Invar alloy nanocontacts

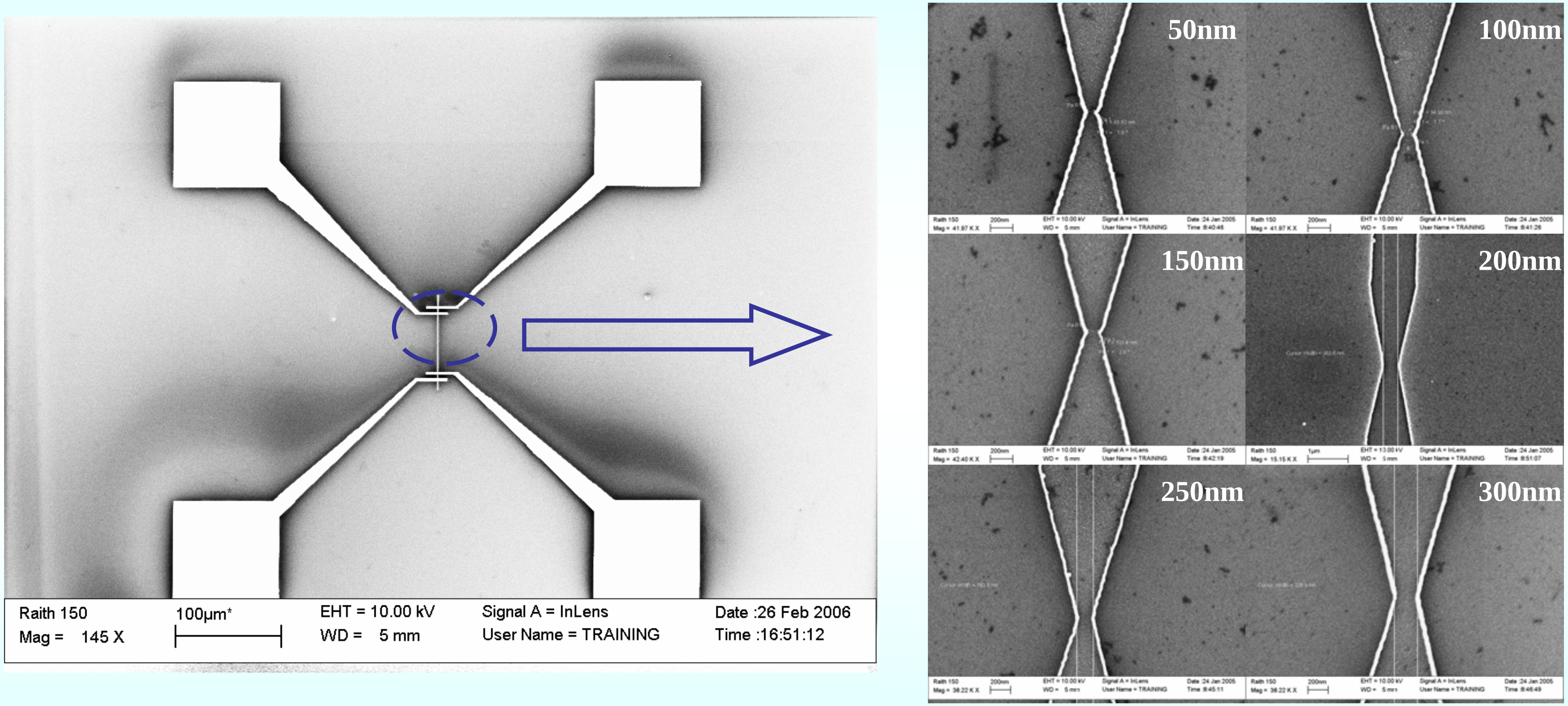

Different widths of Invar alloy nanocontacts and the measurement electrodes

Gu et al. APL 88（2006）033108

Domain wall magnetoresistance

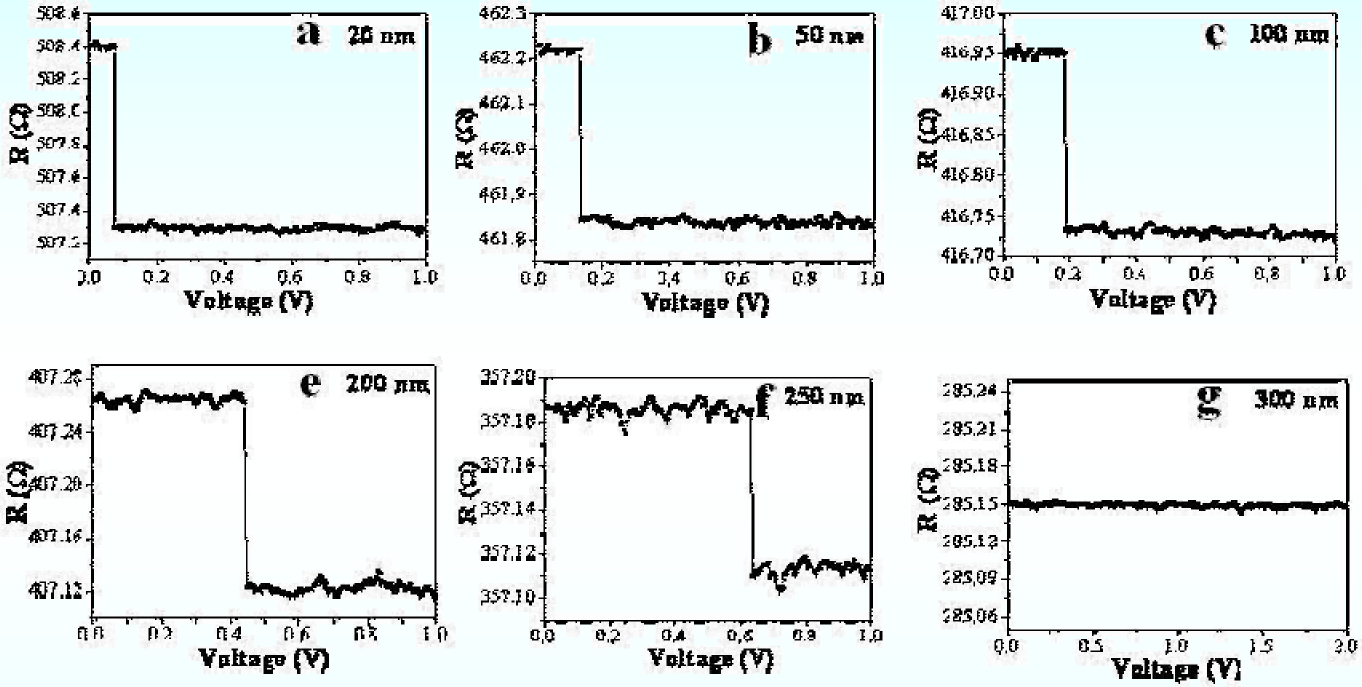

- ➢ **nanocontact can pin a domain wall**
- ➢ **the change of resistance is DWMR**
- ➢ **DWMR decrease with the increasing width**
- ➢ **critical current increase with the increasing width**

Domain wall magnetoresistance

“domain wall displacement by spin polarized current”

L. Berger J. Appl. Phys. 55,1954(1984)

“spin pressure”

J.M.D. Coey Phys. Rev. Lett. 87,026601(2001)

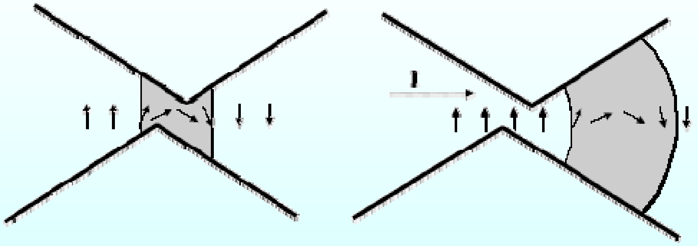

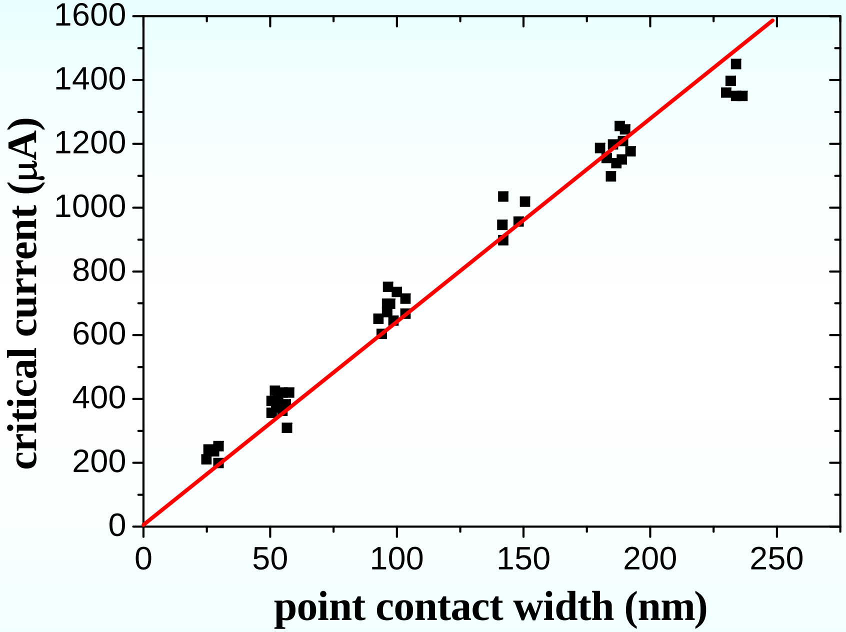

The current density required to be of the order 1.8E7 A/cm^2

(agreement with the observations in bulk materials)

Results in other ferromagnetic metals

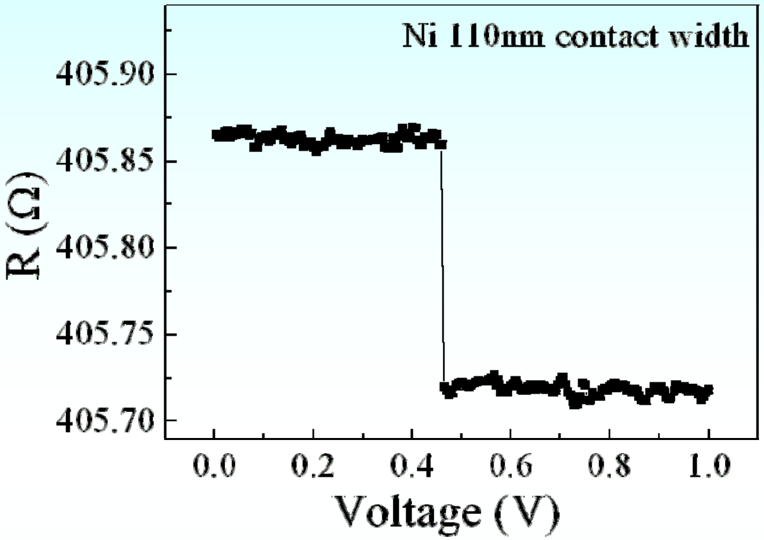

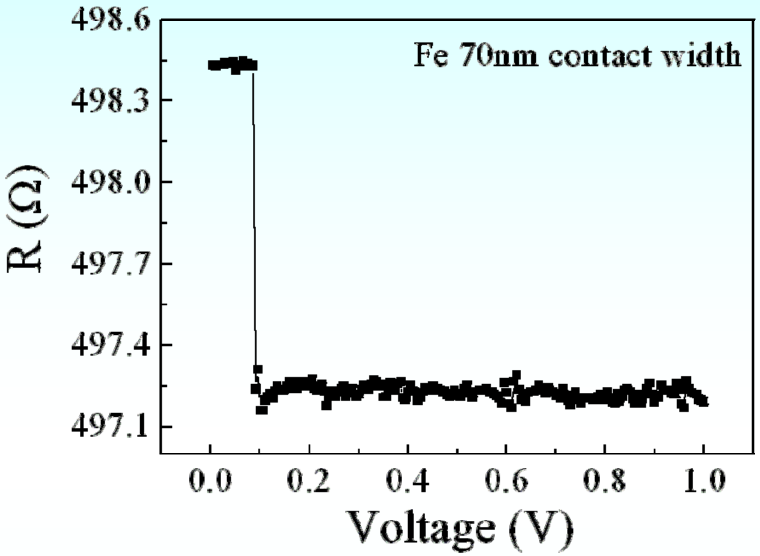

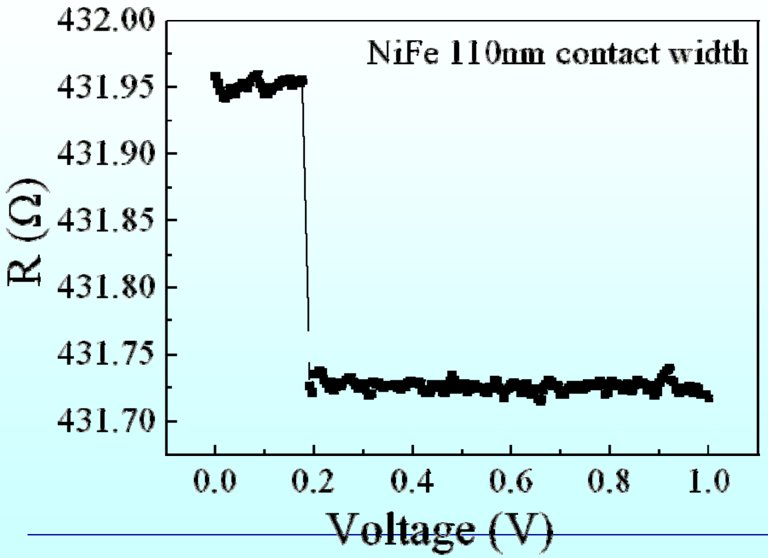

The critical width decreases with the increasing coercive force

Gu et al. Nanotechnology 18（2007）295403

Micro-Magnet Simulation (OOMMF)

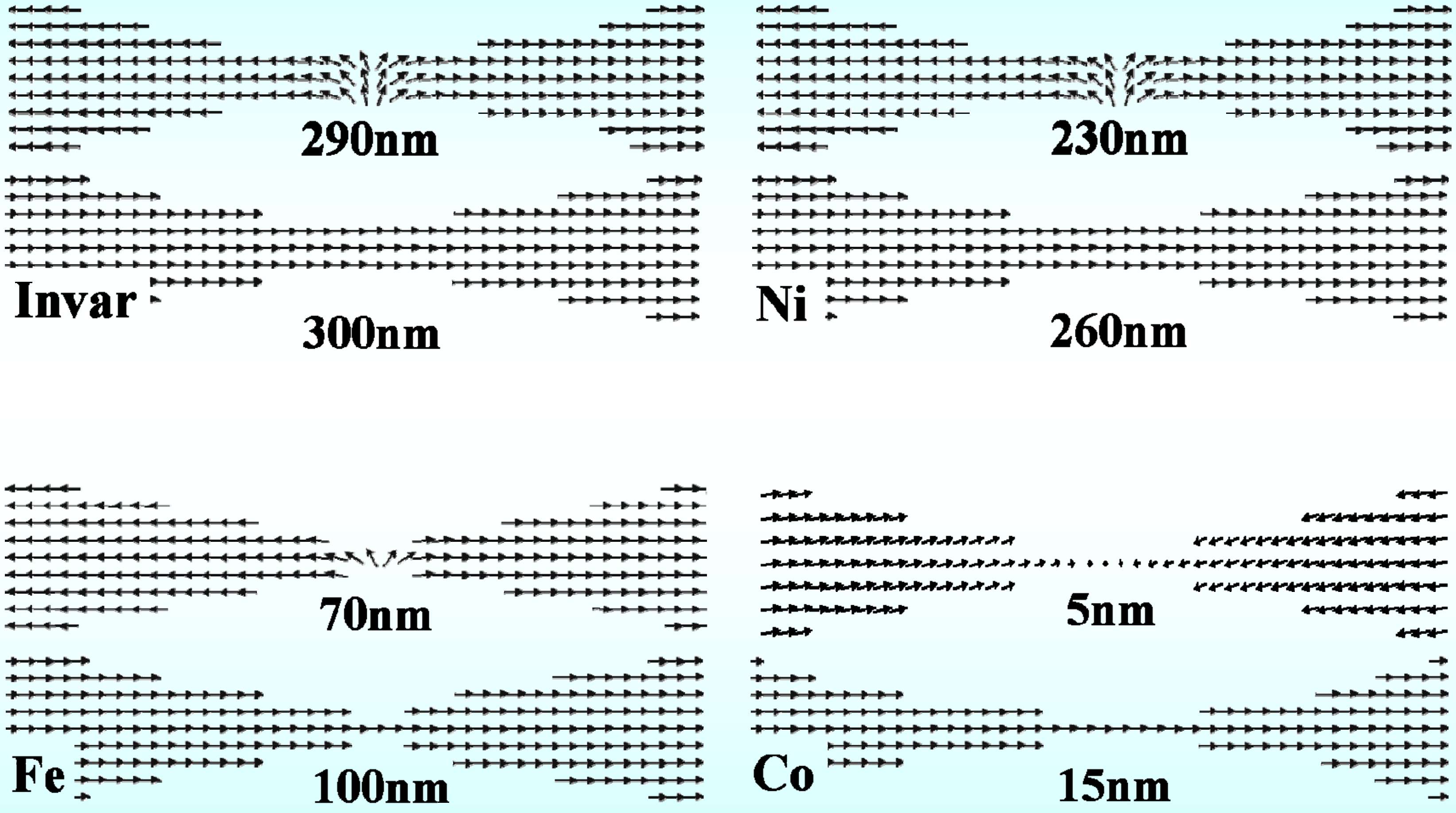

Agreement with above experimental results

Critical current and coercive force

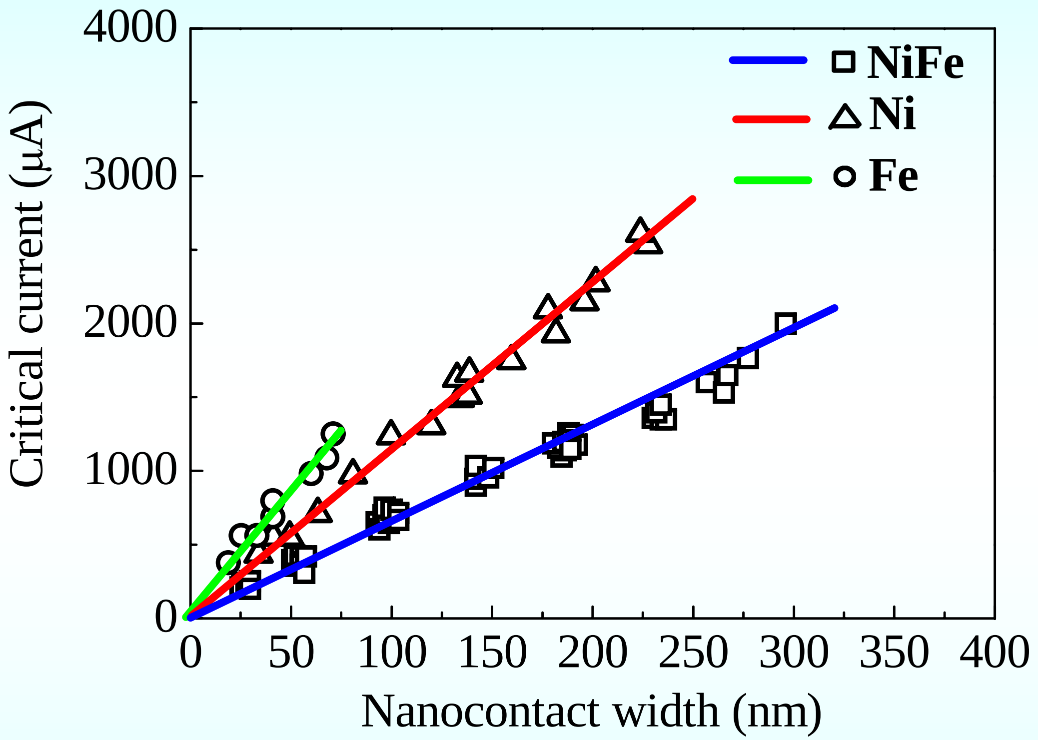

" spin pressure" by spin polarized electron:

$P \propto J\ \tau_{sr}\Delta/e\delta$

Critical depin pressure:

$P=\pi^3 Am/2S$

$J \propto \pi^3 Ame\delta/2S\tau_{sr}\Delta$

NiFe	Ni	Fe	Co
0.05 Oster	0.7 Oster	1 Oster	10 Oster

Critical current increases with the coercive force

The direction of DW motion

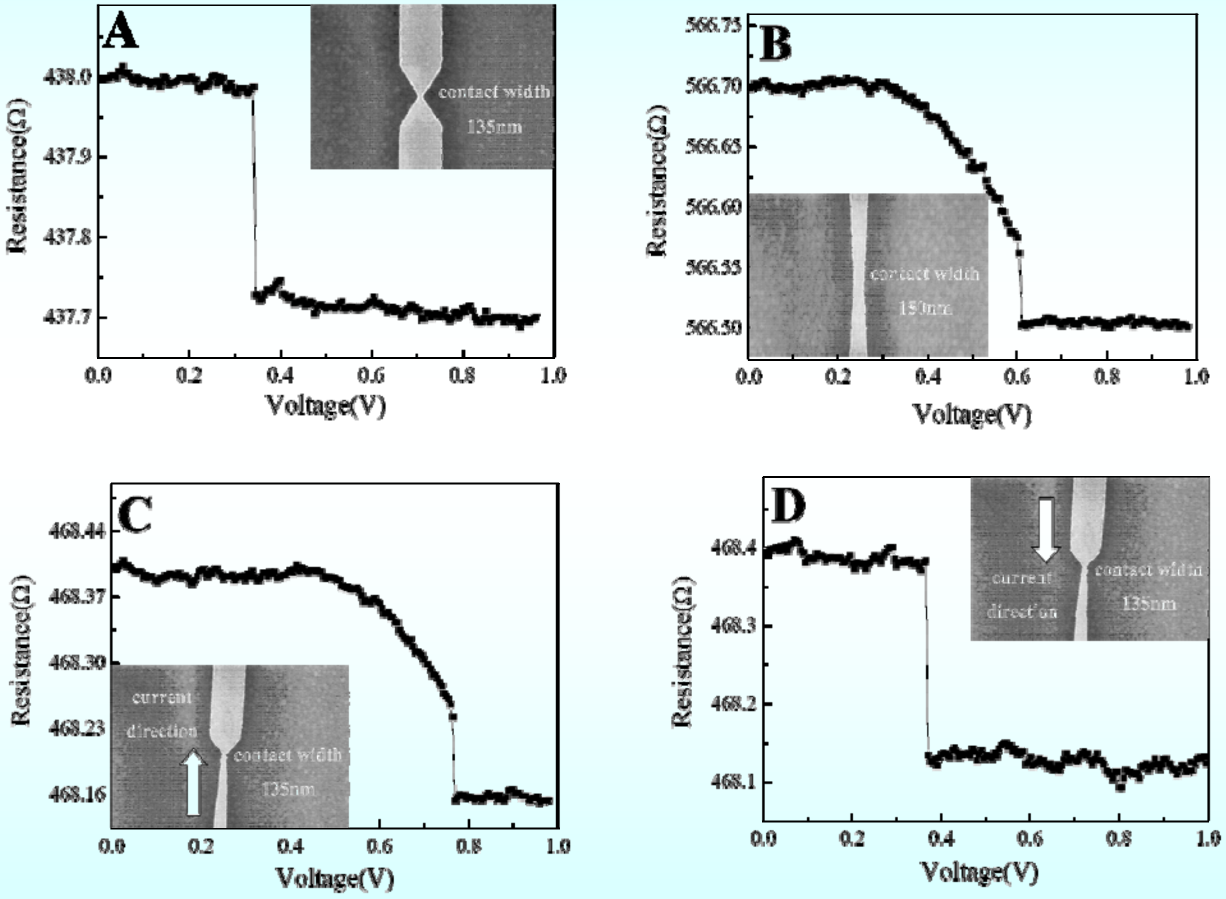

Direction of DW motion is the same to that of current carrier

Resistance change in different structures

Gu et al Nature Nanotechnology 3（2008）97

Alternating Current resistance spectra

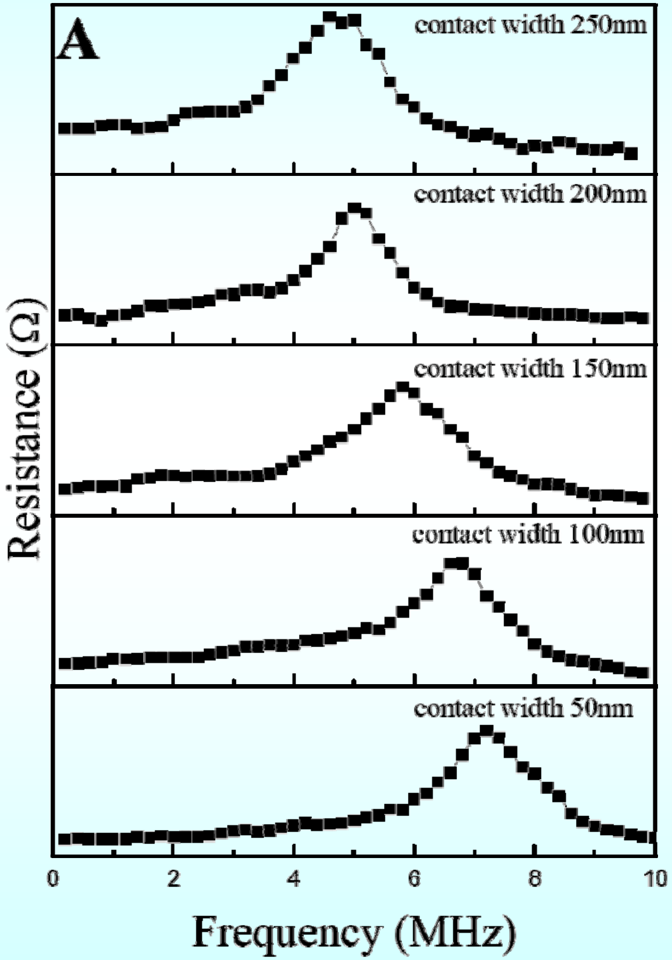

AC voltage near the critical intensity

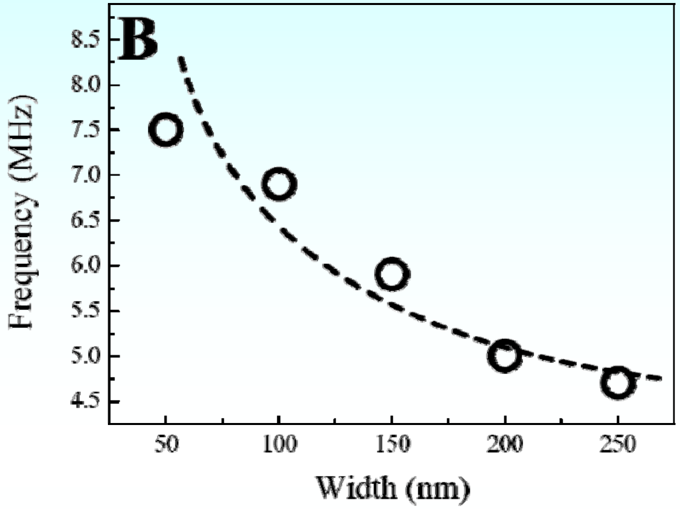

small oscillation

$f^2=k/m$

$m=h^2N/(4\pi^2KW^2)$

$f \sim 1/W^{1/2}$

Contact width is a important parameter for controlling the resonance frequency

Gu et al. Nature Nanotechnology 3（2008）97

Fitting results

$$\Delta\,\mathbf{R}(f) = \frac{1}{8\pi^2 m\tau I^2}\frac{f^2\left|F(f)\right|^2}{\left(f^2-f_e{}^2\right)+\left(f/(2\pi\tau)\right)^2}$$

Eiji Saitoh et al. Nature 432, 203(2004)

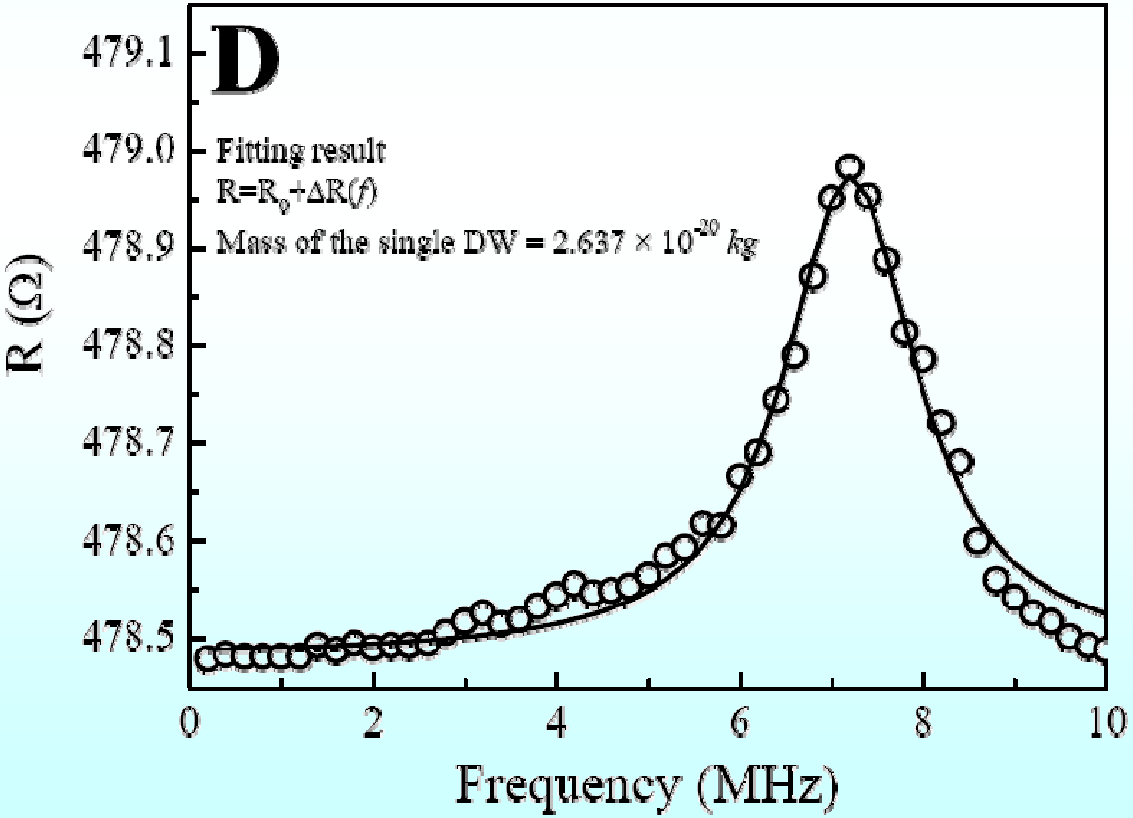

Nowaday Spintronic logic devices

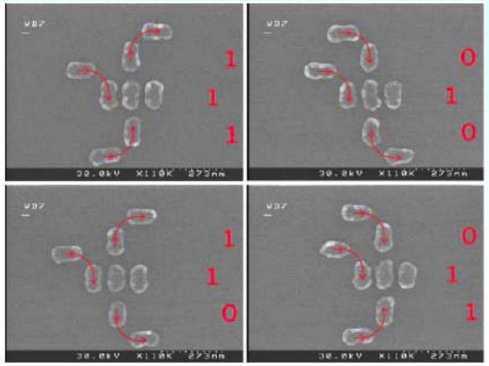

Fig. 3. Majority gates designed for testing all input combinations of the majority-logic operation. The arrows drawn superimposed on the SEM images illustrate the resulting magnetization direction due to a horizontally applied external clock-field. The magnetic state of the AFC inputs has the opposite effective votes on the central magnet as compared with the FC inputs, so AFC and FC inputs are assigned the same logical value for opposite magnetizations. The bit value "0" is assigned to magnetization direction down along the vertical axis of FC input magnets and the central magnet, and value "1" is assigned to magnetization up. The AFC input is defined oppositely.

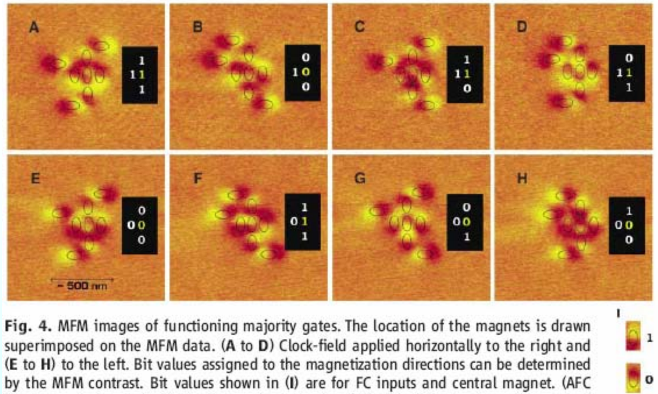

Fig. 4. MFM images of functioning majority gates. The location of the magnets is drawn superimposed on the MFM data. (**A** to **D**) Clock-field applied horizontally to the right and (**E** to **H**) to the left. Bit values assigned to the magnetization directions can be determined by the MFM contrast. Bit values shown in (**I**) are for FC inputs and central magnet. (AFC inputs are designated with the inverse logical values.) The black insets show alignment of magnetic dipoles, accounting for antiferromagnetic and ferromagnetic coupling, and demonstrate correct MQCA majority logic gate functionality.

A.Imre et al. Science 311,205

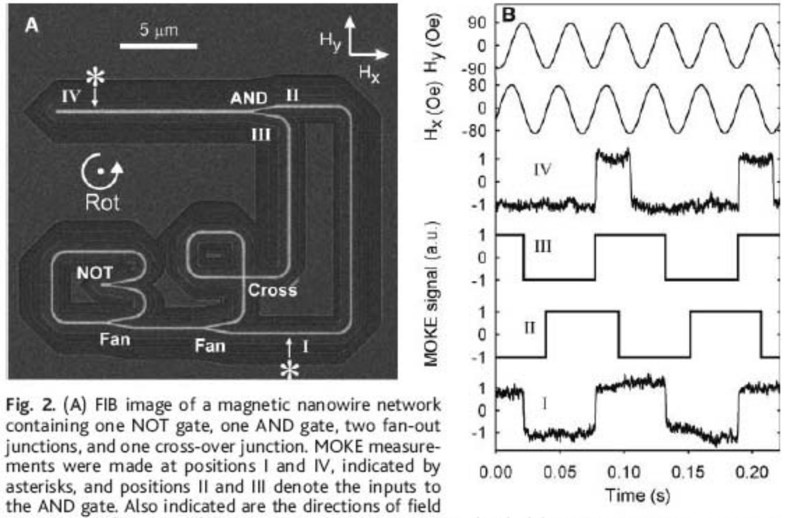

Fig. 2. (A) FIB image of a magnetic nanowire network containing one NOT gate, one AND gate, two fan-out junctions, and one cross-over junction. MOKE measurements were made at positions I and IV, indicated by asterisks, and positions II and III denote the inputs to the AND gate. Also indicated are the directions of field components (H_x and H_y) and the sense of field rotation (Rot). (B) MOKE traces describing the operation of the magnetic circuit within a counterclockwise rotating field with amplitudes H_x^0 = 75 Oe and H_y^0 = 88 Oe and dc offset of H_x^{DC} = −5 Oe. Experimental MOKE measurements from positions I and IV of the circuit are shown. Traces II and III are inferred from trace I and show the magnetization state of the AND gate's input wires.

Cowburn et al. Science 309,1688

Driven by Magnetic field

detected by MFM or MOKE

Not compatible for CMOS circuit

NOT gate circuit

Equivalence circuit

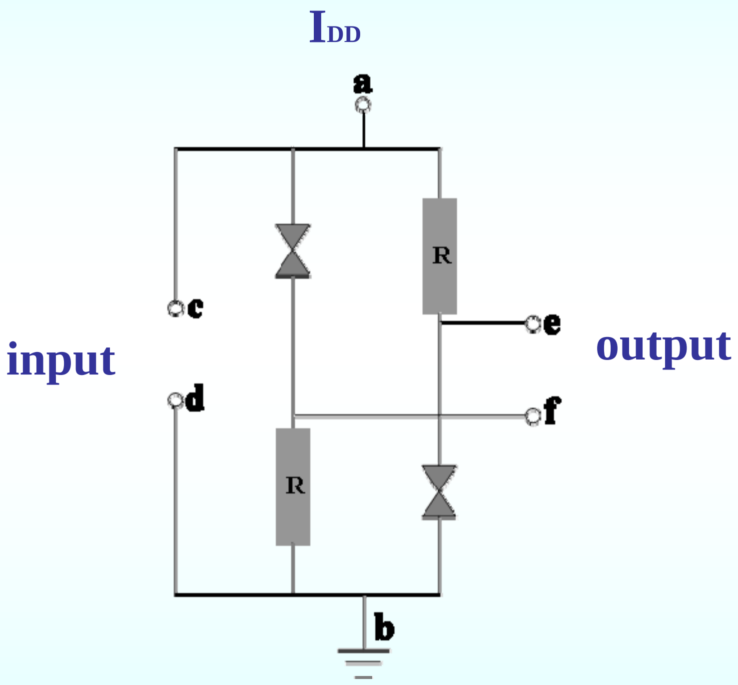

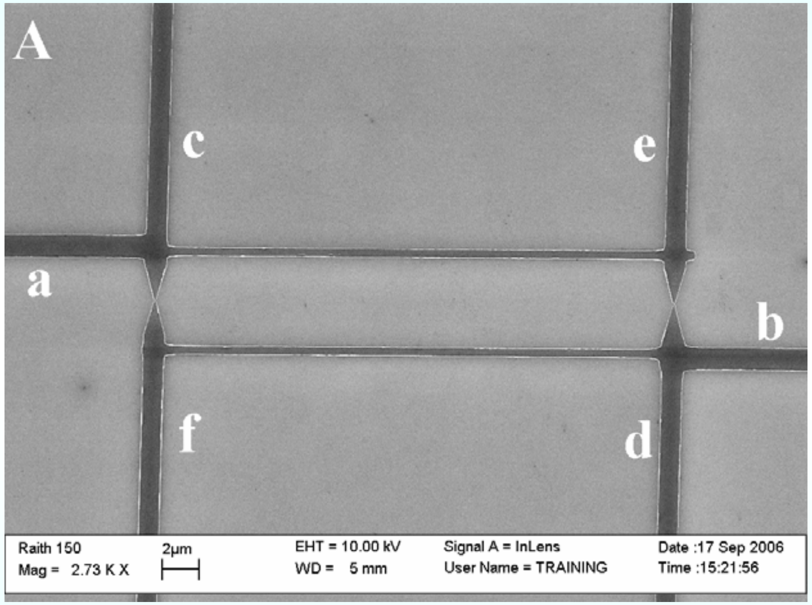

$I_{DD} \approx$ <critical value

$R = R_{\text{low resistance}}$

Gu et al. Nature Nanotechnology 3（2008）97

NOT gate circuit

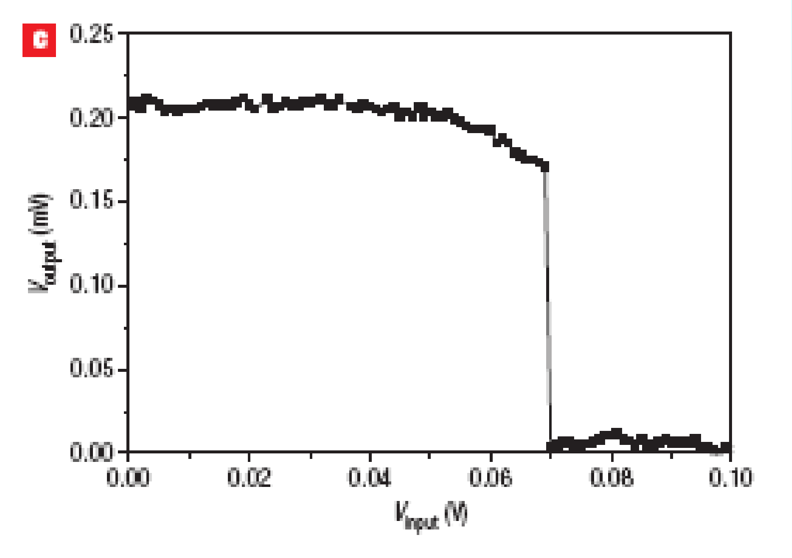

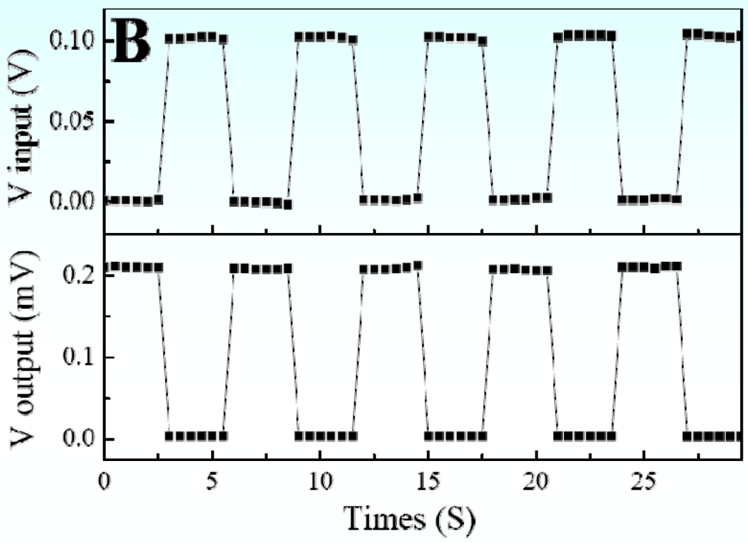

- the intrinsic oscillation frequency of a 50-nm nanocontact is 7.5±0.1 MHz, thus the NOT circuit made from two 50-nm nanocontacts could reach the maximum logic computing speed of 7.5±0.1 MHz.
- the power dissipation could be estimated using the relation $P=VI=1.2\times10^{-4}$ W (where $V=0.24$ V and $I=5.1\times10^{-4}$ A, obtained from experimental data), which is very low compared with that of a Si circuit.

NOT gate circuit

- work at room temperature without the use of an applied magnetic field

- the high carrier densities made possible by the use of metals rather than semiconductors

- the electrical controls should make it relatively straightforward to communicate with standard CMOS circuitry

- the relative simplicity of the circuits should also make it possible to scale the circuits to smaller sizes.

谢谢大家！